[AMERICAN JOURNAL OF SCIENCE, VOL. 299, APRIL, 1999, P. 257–288]

THE DOLOMITE PROBLEM: CONTROL OF PRECIPITATION KINETICS BY TEMPERATURE AND SATURATION STATE

ROLF S. ARVIDSON* and FRED T. MACKENZIE**

ABSTRACT. The mineral dolomite and the uncertainties surrounding its origin have attracted the attention of earth scientists for over a century. The core of the dolomite "problem" is the apparent paradox posed by the paucity of dolomite in modern marine depositional environments versus its relative abundance in the sedimentary rock record. Solving this problem requires knowledge of the conditions under which the mineral forms and the rate of precipitation under those conditions.

As a working hypothesis, it is suggested that the precipitation rate of dolomite may be quantified and modeled in a manner similar to other carbonate minerals through application of a rate law that represents the rate as a simple function of saturation index,

$$r = k(\Omega - 1)^n.$$

This hypothesis is tested in a series of experiments by measuring the steady state rate of dolomite precipitation in a dolomite-seeded flow reactor through analysis of reacted fluid chemistry. By varying temperature from approx 100° to 200°C and saturation index (Ω) from near saturation to ~100, sufficient data were collected to solve for the reaction order and Arrhenius rate constant ($k = A \exp[-(\epsilon_A/RT)]$) of this rate law.

The dolomite produced in these experiments was variable in composition but typically a calcium-rich protodolomite, forming syntaxial overgrowths on the seed material. At the highest supersaturations obtained, formation of distinct nucleation centers was observed. These experiments do confirm a strong temperature dependence for the precipitation reaction (activation energy $\epsilon_A = 31.9$ kcal mol^{-1}) and moderate dependency on saturation index ($n = 2.26$, log $A = 1.05$). The experimental findings of this paper suggest that the abundance of dolomite in the sedimentary rock record reflects, at least in part, environmental changes in temperature and seawater chemistry over geologic time.

INTRODUCTION

The composition and distribution of material in geochemical systems are often strongly controlled by reaction kinetics. This control is especially important at earth surface temperatures, as most chemical reaction rates exhibit a positive temperature dependence. If rates of precipitation, dissolution, oxidation, et cetera, are sluggish, systems may maintain distributions far from thermodynamic equilibrium for geologically significant periods of time. Free energy data now exist for a great many minerals, gases, and aqueous species, making calculation of the distance from equilibrium, that is, the extent of over- or undersaturation of a solution with respect to a given mineral, a straightforward matter. However, without corresponding data for reaction rates, equilibrium calculations may be of little use in predicting actual mineral assemblages.

Marine carbonates and dolomite in particular are good examples of the kinetic control of mineral composition and distribution. Surface seawater is strongly oversaturated with respect to ideal dolomite ($CaMg(CO_3)_2$), and yet there is little evidence of widespread dolomite precipitation in modern, open marine sediments. Modern dolomite does indeed exist but is common only in certain environments: (1) marginal, restricted, hypersaline regimes such as the Coorong lakes of South Australia (Alderman, 1959), supratidal lagoons on the island of Bonaire, Netherland Antilles (Deffeyes, Lucia, and Weyl, 1965), and the sabkhas of the Persian Gulf (Wells, 1962); (2) nonmarine lakes such as Deep Spring Lake in eastern California (Jones, 1961, 1965), and other examples (Graf, Eardley, and Shimp, 1961; Calvo and others, 1995; Anadón and Utrilla, 1993);

* Department of Oceanography, Texas A&M University, College Station Texas 77843
** Department of Oceanography, University of Hawaii at Manoa, Honolulu, Hawaii 96822

and (3) zones of microbial sulfate reduction, in which porewater alkalinity is greatly enhanced over its seawater value, giving rise to so-called "organogenic" dolomite (Baker and Burns, 1985; Compton, 1988; Middelburg, de Lange, and Kreulen, 1990; Kelts and McKenzie, 1982; Vasconcelos and McKenzie, 1997).

Dolomite is also found in environments ranging from the shallow subtidal (Mazzullo, Bischoff, and Teal, 1995) to supratidal (Carballo, Land, and Miser, 1987). Various mechanisms have been proposed to account for the rare occurrence of dolomite in these environments, such as tidal pumping of seawater or mixing of meteoric and marine water (Badiozamani, 1973; Land, 1973; Folk and Land, 1975).

Although there is large uncertainty as to how dolomite forms in modern environments, there is little disagreement that it is at best a very minor constituent of Recent marine sediments. The meager distribution of Recent dolomite contrasts strongly with its common abundance in ancient sedimentary rocks of marine origin, leading to the paradox commonly referred to as the "dolomite problem." Sufficient data regarding the physical and chemical conditions and the rate at which dolomite precipitation proceeds could resolve this problem, and permit an understanding of the true significance of this important mineral in the rock record.

There is a general consensus that the dearth of Recent dolomite reflects a kinetic control, but there are very few measurements of rates of dolomite growth from either field or laboratory settings. Peterson, Bien, and Berner (1963) derived a linear growth rate of $\sim$0.5 Åy^{-1} from the ^{14}C ages of size fractions of dolomite crystals taken from muds of Deep Spring Lake, California. This rate is exceedingly slow, and dolomite crystals growing at this rate would require 200 Ma to acquire an edge length of 1 mm. This result is in great contrast with the observed size of Holocene dolomite crystals forming, for example, in the Florida Keys (Carballo, Land, and Miser, 1987), the Persian Gulf (Baltzer and others, 1994), and the Coorong (von der Borch, Rubin, and Skinner, 1964) of South Australia. In addition, rates cannot be meaningfully compared without simultaneous measurement of prevailing physico-chemical conditions.

In a preliminary effort to place the few laboratory data available into a meaningful framework, Arvidson and Mackenzie (1997) computed dolomite growth rates and solution saturation states from published dolomite synthesis experiments. The relationship between these two independent pieces of information was expressed as a rate law consistent with the hypothesis that the rate of dolomite precipitation is a function of temperature and solution composition. This treatment is similar to that taken with other carbonate minerals, in which the rate is expressed as a simple function of saturation state. Precipitation rates computed from this model agreed closely with age estimates in case studies of sabkha and organogenic dolomite of Recent to Pleistocene age. We also concluded that relatively modest increases in temperature and seawater saturation state could potentially give rise to large increases in the overall rate of dolomite precipitation and a substantial convergence of the relative rates of calcite and dolomite.

The present paper presents an expansion of this initial effort, with the goal of describing how the rate of dolomite crystal growth varies as a function of solution temperature and saturation state. To accomplish this, rates of dolomite crystal growth were measured in a series of laboratory experiments using a circulating seeded reactor at temperatures from $\sim$100° to 200°C. The data were used to constrain the parameters of a parabolic rate law,

$$r = k(\Omega - 1)^n, \tag{1}$$

where Ω is the saturation index of the solution with respect to ideal dolomite ($a_{Ca^{2+}}a_{Mg^{2+}}a^2_{CO_3^{2-}}/K_{T,dol}$), and n is the order of the overall reaction. The rate constant k is assumed to have an Arrhenius form,

$$k = A\, e^{-\epsilon_A/RT}, \tag{2}$$

where A is the so-called pre-exponential term, and ϵ_A is the activation energy. This law can be expanded as

$$\log r = -\frac{\epsilon_A}{2.3\,RT} + \log A + n \log (\Omega - 1). \quad (3)$$

Solving for the free parameters in this law (n, ϵ_A, A) permits calculation of the precipitation rate of dolomite at a given temperature and solution composition.

These experiments differ substantially in method from previous laboratory work on dolomite. The majority of past experiments have been conducted in closed bombs, typically reacting $CaCo_3$ in concentrated $CaCl_2$-$MgCl_2$ solutions under essentially hydrothermal conditions to form dolomite. To be successful, however, this approach demands that relatively large amounts of dolomite form, rendering detection of small extents of reaction problematic. It is further handicapped by uncertainty of the in situ distribution of solution components under the higher temperature conditions of the reactor itself. Analysis of earlier literature data and their application to the present model were described in Arvidson and Mackenzie (1997). In more recent work, Malone, Baker, and Burns (1996) observed that the rate of recrystallization of initially disordered (Ca,Mg)-carbonates was a strong function of temperature, and temperature increases produced corresponding increases in $MgCO_3$ and cation ordering. In adsorption experiments at room temperature and fixed pCO_2, Brady, Krumhansl, and Papenguth (1996) concluded that dehydration and carbonation of magnesium was the most probable rate-limiting step at low temperatures.

Data available from the literature suggest that dolomites synthesized at temperatures less than ~200°C are often calcium-rich and imperfectly ordered. It should be emphasized that these materials, despite their metastability, are distinct from magnesium calcite, and this was the purpose of Graf and Goldsmith's (1956) original introduction of the term protodolomite. It should also be pointed out that although patient experimentalists have not succeeded in synthesizing dolomite at room temperature (Land, 1998), the total duration of such experiments is still very short compared to the age of Recent dolomite forming, for example, in the Abu Dhabi sabkha of the Persian Gulf or the Coorong lagoons of South Australia. In fact, the results of our experiments suggest that laboratory synthesis of dolomite at ~25°C is probably not feasible.

METHODS

Reactor design and analytical methods.–The reactor used in these experiments is similar in design to flow reactors used in solubility and kinetic studies of other minerals and is capable of measuring slow precipitation reactions at moderately elevated temperature and confining pressure. Our general objective was to measure the rate of dolomite precipitation over a sufficient span of temperature and solution composition to resolve the relationship between precipitation rate, temperature, and saturation state. To accomplish this goal, a solution supersaturated with respect to ideal dolomite was circulated at a fixed rate over dolomite seeds of known surface area in a modified plug flow reactor.

In a steady-state plug flow reactor, fluid flows in one end of the reactor vessel, interacts with the reactor contents in a single pass, and exits. This system can be described by (Levenspiel, 1972)

$$\frac{V}{v_0} = \int_{c_0}^{c_f} \frac{dc}{-r}. \quad (4)$$

V, v_0, c_0, c_f, and r denote reactor volume, volumetric input (= output) flow rate, and input and output concentrations of a component consumed in a reaction having rate r, respectively. The left hand quantity is the residence time of the reactor. The necessity of integrating the rate function in the right hand side of eq (4) is avoided through introduction of a recycle circuit as shown in figure 1. The ratio of the volumetric flow rate of recycled fluid v_1 and that exiting the system v_0 is represented by R,

$$R \equiv \frac{v_1}{v_0}.$$

Reactant concentration and flow rate prevailing at the immediate inlet to the reactor (c_2, v_2) represent the sum of the return (c_f, v_1) and input (c_0, v_0) flows. We solve for c_2 in

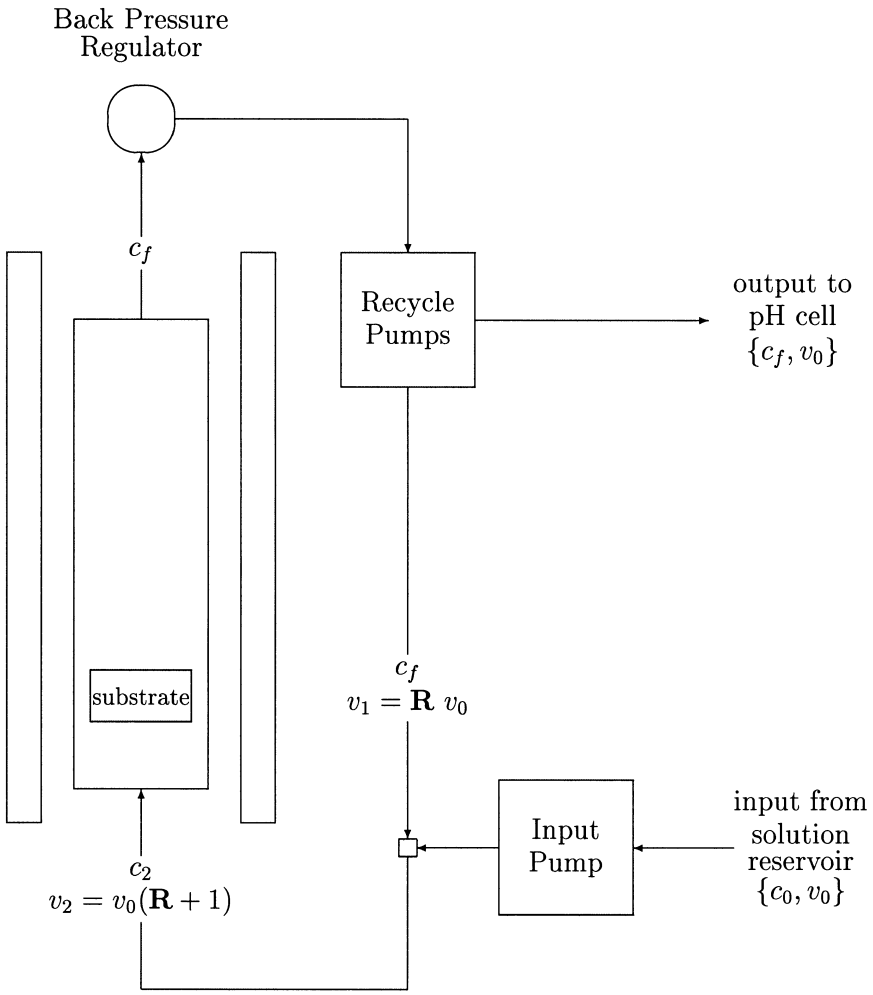

Fig. 1. Schematic representation of hydrothermal flow reactor. Volumetric fluid flows are denoted by v_0 (system input), v_1 (recycled), and v_2 (reactor input); fluid compositions are labeled c_0 (system input), c_f (output), c_2 (reactor input). Output flow composition c_f is equivalent to that of the in situ reactor fluid providing that the ratio of recycled flow to input flow rate, $R \equiv v_1/v_0$, is large.

terms of the observable quantities R, c_0, c_f:

$$c_2 = \frac{Rc_f + c_0}{R + 1}.$$

The volumetric flow at the immediate inlet to the reactor (v_2) is the sum of the recycle and input flows ($v_1 + v_0$). By substitution,

$$v_2 = v_0(R + 1).$$

By using c_f and c_2 as outlet and inlet boundary conditions, the basic equation for this recycle reactor is

$$\frac{V}{v_0} = (R + 1) \int_{Rc_f + c_0/R+1}^{c_f} \frac{dc}{-r}. \tag{5}$$

In the limit of large R, eq (5) simplifies to

$$\frac{V}{v_0} = \frac{c_f - c_0}{-r}. \tag{6}$$

Thus by increasing the recycling rate, the reaction rate may be calculated as a simple difference of input and output concentrations. Precipitation rates are expressed in units of moles cm^{-2} s^{-1} by normalizing eq (6) with respect to the total reactive surface area of seed material (S, hereafter assumed equivalent to total surface area) per unit reactor volume,

$$-r = \frac{\Delta c \cdot v_0}{S}.$$

The experimental setup consists of an input pump, reaction vessel, pressure and temperature regulators, recirculation pumps, and pH electrode cell (fig. 1). The reactor proper consists of a tubular titanium vessel fitted with permanent upper and lower removable frits (2 μm pore size) that confine the solid dolomite seed material. Pressure connections at both ends of the reactor tube consist of cone fittings and tubing adapters held in place by threaded collars. The top collar accepts a short coupling tube, surmounted by a large cross that contains pressure gauge, thermocouple, and fluid exit ports and adapters.

All wetted parts of the reaction vessel proper, including frits, compression rings, upper coupling tube, and lower adapter are composed of commercial titantium alloy (Ti4A16V, High Pressure Equipment Corporation). Fluid is introduced into the system by the input pump ($v_0 \sim 0.2$ to 0.7 mL min^{-1}). Fluid arrives at the base of the reactor after transit through a preheater circuit consisting of Hastelloy-C tubing coiled around the length of the reactor. The reaction vessel and preheater circuit reside within a tubular ceramic furnace. Temperature is measured by a thermocouple ('E'-type chrome-constantan with Inconel sheath) fitted in the reactor flow stream such that is grounded junction sits immediately above the upper frit. Initial testing of the reactor by mounting surface thermocouples showed thermal gradients of less than 1°C over the reaction volume during recycle operation at temperatures up to ~200°C. Thermocouple output is measured by a pen recorder and microprocessor-controlled relay that in turn controls furnace output. Fluid exits the reactor through a short cooling loop and is received by a gas-loaded back pressure regulator that fixes the confining pressure of the system.

After leaving the high pressure regulator, reacted fluid passes through an in-line titanium filter and enters a low pressure circuit (⅛ inch PEEK tubing and fittings) through

which it either exits the system or enters the recycle circuit. Pressure in this area is maintained at ~100 psi by a smaller in-line back pressure regulator to suppress possible boiling and recycle pump input valve cavitation. Exiting fluid is delivered through thick-walled microbore Teflon tubing and a 0.22 μm filter to a 25°C pH cell and collected for analysis as described below. Two dual-piston high pressure reciprocating pumps (1/8 inch pistons) return fluid to the reactor at a cumulative rate of ~20 mL/min, yielding a maximum recycling ratio of ~100. Total system volume is ~60 mL.

Experiments were conducted by loading the reactor with approx 5 g of seed dolomite. The system is initially purged with deionized water and allowed to reach run temperature. Operating temperatures of ~150°C are reached in approx 20 to 30 min; temperatures of ~200°C require about 1 hr. Typically the system was run at temperature with pure water for 12 hrs prior to introduction of stock input solutions. This delay served two purposes. First, the approach to run temperature typically exceeded the setpoint target and oscillated somewhat, until operating thermal gradients of components downstream of the reactor volume were established. Temperature overshoots in the presence of reactant solutions supersaturated with respect to unwanted carbonate phases (for example, calcite) could result in their nucleation. Introduction of reactant solutions was thus delayed until stable run temperatures had been achieved. Second, this delay served to homogenize and prepare the seed surface by minimizing soluble artifacts.

Input solutions are diluted mixtures of reagent grade stocks of $CaCl_2$, $MgCl_2$, and $NaHCO_3$. The solution was contained in a large carboy bubbled with a CO_2-N_2 mixture. Gas mixing was accomplished in a calibrated dual tube rotameter fitted with precision needle valves. Selection of appropriate diameter tubes and float densities thus provided a wide range of possible pCO_2 values. The gas mixture was saturated by bubbling initially through deionized water prior to introduction into the input solution carboy.

Fluid output samples were collected over intervals of about 4 hrs of reactor run time. The overall duration of each run was dictated by the time necessary to reach a steady state rate. This "induction period" was variable in duration, ranging from 12 to 48 hrs, with little apparent relation to the conditions of the experiment. Once steady state behavior was achieved, the reaction rate was calculated by averaging output concentrations over at least 24 hrs of reaction operation.

Hydrogen ion activity was measured prior to sample collection with a Corning model 350 pH meter and combination glass electrode mounted in a specially designed 25°C plexiglass flow cell. The cell volume and electrode membrane were closed with respect to the atmosphere, although a small head space was maintained within the cell to act as a bubble trap and to minimize any effects due to differential fluid pressure on the electrode itself. The electrode was calibrated by loading pH 4 and pH 7 NIST-traceable buffers into the cell at the beginning of a sample collection period and recalibrated after sample collection was complete. Both input and output solution pH could be measured in this manner. Corrections due to drift in the electrode's calibration were made by assuming the slope and intercept to be linear functions of time t, and interpolating pH(t) appropriately. Only during instances of obviously poor electrode performance was this correction significant.

Both input (unreacted) and output (reacted) solutions were titrated for total alkalinity, total dissolved calcium, total alkaline earths, and total chloride. Total alkalinity (versus total carbon) and pH were chosen as carbon system constraints because of substantial gas phase separation observed in the fluid sample, especially apparent when gas-tight syringes were employed to collect fluid. This was due both to the length of time required to retrieve a sufficiently large volume of sample for analysis and the high CO_2 fugacities of most of the experiments. This loss of dissolved CO_2 has no effect on total alkalinity, whereas trial coulometric titrations of syringe-collected samples showed up to 20 percent loss of the total disolved carbon calculated from inline pH and alkalinity.

Although some initial gas evolution would also occur in the head space overlying the electrode in the pH cell, this small volume rapidly equilibrated with the output fluid, as could be seen by monitoring pH after assembly of the cell. Once equilibrated, the pCO_2 of this headspace volume should essentially reflect saturation with respect to the dissolved CO_2, and accurate pH measurements and downstream fluid recoveries could begin. In addition, because of their sensitivity to changes in the state of the system, pH and alkalinity data were often used as indicators of a steady state reactor condition.

The errors attending these analyses and thus their contribution to the calculation of the rate represented by a given sample are relatively small (table 1). In virtually all the data presented, rates are calculated either on the basis of changes in total alkalinity or total divalent cations. If the overall precipitation reaction proceeds as

$$Ca^{2+} + Mg^{2+} + 2\ CO_3^{2-} \rightarrow CaMg(CO_3)_2,$$

then the change in total dissolved cations (in equivalents) must also be attended by an equal change in total alkalinity. Although the precision in total alkalinity measurements was often poorer ($\sim$0.3 percent) than that of total divalent cations ($<$0.1 percent), most experiments were conducted in solutions whose total cation concentration was an order of magnitude greater than the total alkalinity. For example, a loss due to reaction of 100 µmoles/kg in divalent cations ($\sim$1 percent of total) would be met with a corresponding change in alkalinity of 200 µeq/kg (20 percent of total). This leverage often made total alkalinity the quantity of choice in rate calculations.

Seed material was prepared from large cleavage rhombs of a metamorphic grade vein dolomite from Selsvann (Aust Agder county) Norway, obtained from Ward's Natural Science Supply. Preparation consisted of separation of the 212 to 500 and 90 to 212 µm fraction by grinding and sieving under acetone, followed by brief washing in 10 percent HCl, final rinsing in distilled water, and drying at 60°C.

Acid washing prior to reaction resulted in dissolution in the form of rounding of interfacial angles, subhedral boundaries, and development of etch pits (fig. 2). Aside from those grains that had suffered obvious fracture, most displayed good rhombic cleavage and well developed cleavage surfaces. Many surfaces were essentially devoid of noticeable topographic features other than a more or less evenly distributed population of etch pits. This lack of surface development made identification of growth features in reacted grains straightforward.

Seed materials were analyzed in a SCINTAG PAD-V automated X-ray diffractometer using Cu-Kα radiation. Samples were prepared as powder smears by grinding under acetone and mounting on zero-background slides. Diffraction data were collected in step

TABLE 1

Analytical methods and errors of analysis

Analyte	method	error
hydrogen ion activity	combination glass electrode	$\pm$0.01 pH units
total alkalinity	acidimetric-Gran	
($\gtrsim$ 2 meq kg^{-1})		$\sim$0.1%
($\lesssim$ 1 meq kg^{-1})		$\sim$0.3%
calcium	potentiometric-EGTA	$<$ 0.1%
magensium (total divalent cations)	colorimetric-EDTA	$<$ 0.1%
chloride	potentiometric-$AgNO_3$	$<$ 0.1%

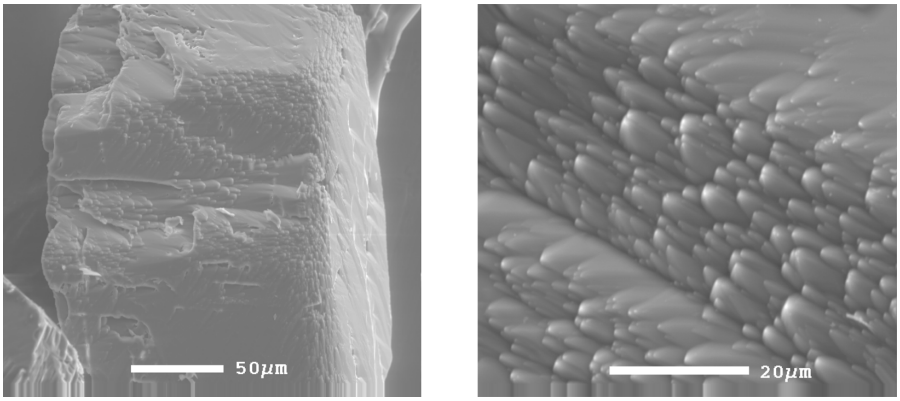

Fig. 2. Unreacted acid-washed seed dolomite, run Ti10. Left: Note formation of etch pits, relatively smooth surfaces, and edge rounding. Grain is typical of seed material used in all experiments. Scale bar 50 μm. Right: Detail indicates probable minimization of excess surface energy through rounding of crystallographic features. Scale bar 20 μm.

scans of 0.02° 2Θ steps, scanning at 2 to 5 sec per step to minimize background noise. The computed d-spacing of the primary $\{10\bar{1}4\}$[1] and secondary diffraction peaks agreed with the entry for ideal dolomite obtained from the JCPDF database to the precision of the instrument. For analysis of reacted samples where the accuracy of absolute peak positions was critical, fluorite (~10 wt percent) was added as reference material. The presence of strong and well-defined principal superstructure reflections in the seed material indicated a well-ordered dolomite phase.

Seed materials and reaction products were also examined under a Zeiss Model AG350 electron microscope equipped with secondary and backscatter electron detectors and energy-dispersive (EDS) spectrometer. The composition of unreacted seed materials was determined by extensive EDS analysis and indicated a very homogeneous and essentially perfect 1:1 ratio of Ca to Mg. These data agreed with additional EGTA/EDTA determinations of Ca and Mg in the seed dolomite. It should be noted, however, that EDS provides only a semi-quantitative estimate of elemental composition (the instrument used an internal calibration which was checked against the Ca and Mg composition of seed dolomite grains at sites where topographic artifacts were minimized). SEM imaging also indicated a trace contribution of Fe and Mn in the form of oxide and silicate inclusions. These inclusions were not observed in reacted grains and presumably dissolved during reaction. These trace phases may also have been the source of a single, very low intensity diffraction peak (essentially at background) observed in unreacted grains and absent in reacted samples. Samples retrieved after lengthy reaction times at high temperatures were also typically discolored with small flecks of material. SEM/EDS analysis indicated these to be μm-sized particles of Fe, Ni, or Cr, probably contributed from the preheater tubing loop. The effect of these contaminants on any reaction kinetics is unknown; however, there was no indication from surface imaging that they interfered with growth of new material. ICP-ES analysis of reacted solutions from a single run at 150°C could not detect these elements.

Surface area was estimated geometrically from SEM images. In addition, specific surface area of selected samples was analyzed by Micromeritics Laboratory, Norcross, Georgia, using single point BET analysis, with Kr gas as the adsorbate gas.

[1] All [hkil] notations are made with respect to the hexagonal unit cell.

High temperature equilibria.–In order to relate measured rates of precipitation to mineral saturation index, an aqueous model was developed appropriate to computing ionic activities and speciation under the conditions that prevail in situ within the reactor volume. Of obvious importance is the accurate representation of the carbonic acid system at temperature, from pH and total alkalinity measured at 25°C. This is accomplished through detailed balancing of all solution components, including total hydrogen ion and water, as described in Reed (1982). Other relevant aspects of this computer-driven ion association model include the ability to introduce arbitrary constraints of saturation state with respect to minerals and gases of interest and compute the mass transfer between solid and gaseous reservoirs necessary to maintain these constraints; the use of an internally consistent thermodynamic database for mineral solubility and dissociation of aqueous complexes computed from free energy data generated largely by the program SUPCRT92 (Johnson, Oelkers, and Helgeson, 1992), incorporating the revised HKF thermodynamic formalism (Helgeson, Kirkham, and Flowers, 1981; Tanger and Helgeson, 1988; Shock and others, 1992), for the temperature and pressure of interest. The equilibrium activities of dissolved components (H^+, H_2O, Na^+, HCO_3^-, Ca^{2+}, Mg^{2+}, Cl^-) is found through iterative solution of the following simultaneous equations:

$$-\overline{M}_i + n_w \left\{ m_i + \sum_j^{N_j} \frac{C_{ij}}{\gamma_j K_j} \prod_h^{N_i} (m\gamma)_h^{A_{hj}} \right\} + \sum_k^{N_k} B_{ik}\varphi_\kappa = 0, \quad i = 1,N_i$$

with optional constraints,

$$-K_k a_k + \prod_i^{N_i} (m\gamma)_i^{B_{ik}} = 0, \quad k = 1,N_k \tag{7}$$

A description of the terms in eq (7) is given in table 2.

TABLE 2

Parameter list for equilibrium model described by eq (7). Basis components are chosen such that their total number is the minimum required to describe completely the system's composition at a given temperature and pressure; they are denoted by indices **h** *or* **i**. *Note that hydrogen ion is included as a basis component, and "total hydrogen" is used to constrain pH at temperature (Reed, 1982; Reed and Spycher, 1984). Aqueous complexes, denoted by* **j**, *comprise those species whose concentration depends entirely on that of basis components. Mineral or gas phases may be introduced as compositional constraints, and are denoted by* **k** *indices*

Symbol	Quantity
N_i	total number of basis components
N_j	total number of complexes
N_k	total number of minerals or gases of interest
$\overline{M}_i$	total moles of the i^{th} component
m_i	molality of the i^{th} free, uncomplexed component
n_w	total kilograms of solvent water
γ	single ion activity coefficient for basis ions or complexes
K_j	equilibrium constant of the j^{th} complex
K_k	equilibrium constant of the k^{th} mineral or gas
φ_k	total moles of k^{th} mineral or gas added to satisfy equilibrium constraints
a_k	activity (or fugacity) of the k^{th} mineral (or gas)
$\mathbf{A}_{hj}$	stoichiometric matrix relating the composition of the j^{th} complex to the h^{th} basis component
$\mathbf{C}_{ij}$	identical to $\mathbf{A}_{hj}$ except when total alkalinity is used as a carbon constraint
$\mathbf{B}_{ik}$	stoichiometric matrix relating the composition of the k^{th} mineral or gas to the i^{th} basis component

CARBONATE MINERAL GROWTH

Dolomite.–The precipitation experiments ranged in temperature from 115° to 196°C, using solutions having variable mixtures of $CaCl_2$, $MgCl_2$, and $NaHCO_3$ under various pCO_2 atmospheres. The original dolomite seed grains retrieved from the reactor after these experiments showed clear evidence of precipitation of new material of dolomite composition. The composition, texture, and extent of development of this new phase was variable. To some extent this variability could be related to the conditions of the experiment, as described below. Coprecipitated phases, including calcite, magnesian calcite, and magnesite ($MgCO_3$), were also identified by SEM/EDS and XRD. The appearance of these phases is confirmed by reacted fluid chemistry. A summary of the experimental runs appears in table 3.

The spatial distribution of visible growth on reacted grains was variable, with many surfaces showing obvious and extensive modification, compared with only minor development along adjacent surfaces of the same grain. The most salient distinction to be made was whether new dolomite had formed as a result of syntaxial or epitaxial growth. Syntaxial growth appears essentially as the migration of steps, progradation of existing crystal faces, and development of complex surface frameworks. In contrast, epitaxial growth appears as the development of distinct crystal nuclei, although the orientation and distribution of growth units may occur in a regular pattern suggestive of control by the underlying substrate. Syntaxial growth of new dolomite predominates in all samples except those reacted at high supersaturation, where it is also accompanied by coprecipitated phases (magnesian calcite and magnesite). These two modes of growth are discussed separately below.

Characteristic styles of syntaxial growth from run Ti10 (170°-196°C) are shown in figure 3. Growth was most commonly developed as thinly aggregated terraces (fig. 3, top row). Lateral migration of steps was apparently favored along certain crystallographic faces, creating an irregular face of step edges in various stages of advancement (fig. 3, bottom left). EDS analysis of these areas showed them to range from 52 to 59 percent $CaCO_3$ in good agreement with the range of data from fluid chemistry. In addition, grain boundaries previously compromised and rounded by etching became sites for reconstruction through advance of steps toward the intersection of crystallographic faces (fig. 3, bottom right).

In experiments supersaturated with respect to calcite and dolomite (run Ti12, 150°C), unique intergrowths of dolomite, magnesian calcite, and essentially pure calcite were observed. The composition of individual growth layers is distinguished by EDS data. These differences in mineralogy are also apparent to some extent from differences in contrast in backscattered electron images (fig. 4). Fluid chemistry data confirm development of essentially pure calcite during certain phases of this experiment.

Samples reacted at high supersaturation with respect to dolomite ($\log\Omega \sim 2$, run Ti01, 150°C) showed surface nucleation of other carbonate phases as well. The development of new heteronuclei on seed material surfaces is shown in figure 5, having compositions of magnesite, magnesian calcite, and dolomite. Growth of magnesite proceeds by the nucleation of submicron rhombic crystallites, often exhibiting irregular or curved faces (fig. 5, bottom right). This experiment (run Ti01) is the only one in which magnesite developed, and magnesite was observed only epitaxially, that is, not in apparent crystallographic continuity either with the dolomite substrate or dolomite phase overgrowths thereof. In contrast, epitaxial growth of dolomite and magnesian calcite appears to begin with the development of irregular submicron particles that coalesce to form larger rhombs. These rhombs can be seen in various intermediate stages of development, with irregular edges and faces forming prior to subsequent infilling (fig. 5, bottom left). Backscatter SEM also shows some contrast between newly crystallizing

TABLE 3

Composition of experimental solutions. All concentrations are given in moles/kg-H_2O. Units of precipitation rate are mols cm^{-2} s^{-1}. Concentrations given in italics indicate those used to calculate the rate

run	T °C	P bars	days	A_T	Ca^{2+}	Mg^{2+}	Cl^-	Na^{+*}	pH	mol% Ca	log rate
ss08	115	109	1.9	0.001057	*0.009679*	*0.043647*	0.107394	0.001798	7.045	41.5 ± 9.6	-10.997
ti01†	150	123	4.4	0.001740	*0.011534*	0.046203	0.116693	0.002959	5.775		-9.786
ti02	150	108	3.8	*0.001291*	0.011734	0.014208	0.052550	0.001958	5.581	75.4 ± 9.3	-11.685
ti03‡	125	113	4.9	0.001719	0.011689	0.046649	0.116891	0.002143	5.541	53.0	
ti04‡	100	48	8.4	0.002236	0.011950	0.045407	0.114460	0.001983	5.741		
ti05§	150	48	6.6	*0.000764*	0.009754	0.003291	0.025398	0.000942	5.862		-12.037
ti06	150	48	5.5	*0.000936*	0.009661	0.009923	0.039253	0.001020	5.600	65.9 ± 5.9	-12.514
ti08	150	48	6.9	0.000824	*0.009648*	*0.009707*	0.038628	0.000743	5.341	61.1 ± 3.2	-11.978
ti09	150	48	8.0	0.000687	*0.009533*	*0.009725*	0.038695	0.000851	5.333	55.3 ± 6.0	-11.623
ti10-196	196	48	2.0	*0.000548*	0.009440	0.009766	0.038815	0.000951	4.875	55.9 ± 3.7	-11.4556
ti10-186	186	48	4.1	*0.000743*	0.009448	0.009792	0.038782	0.001043	4.858	62.5 ± 8.7	-11.697
ti10-180	180	48	3.8	*0.000885*	0.009517	0.009829	0.038814	0.001006	4.937	58.4 ± 4.8	-12.01
ti10-176	176	48	1.8	*0.000908*	0.009491	0.009800	0.038676	0.001004	4.920	59.9 ± 1.8	-12.099
ti10-170¶	170	48	3.2	0.001063	0.009554	0.009861	0.038819	0.001052	5.047	72.1	
ti11‖	135	48									
ti12‖	150	48									

*Sodium concentration computed by balance.
†Magnesite coprecipitate.
‡Dissolution, possibly incongruent.
§Poor analytical precision and balance.
¶Dissolution wrt alkalinity; negligible uptake of M^{2+}.
‖Variable concentrations, data are not presented .

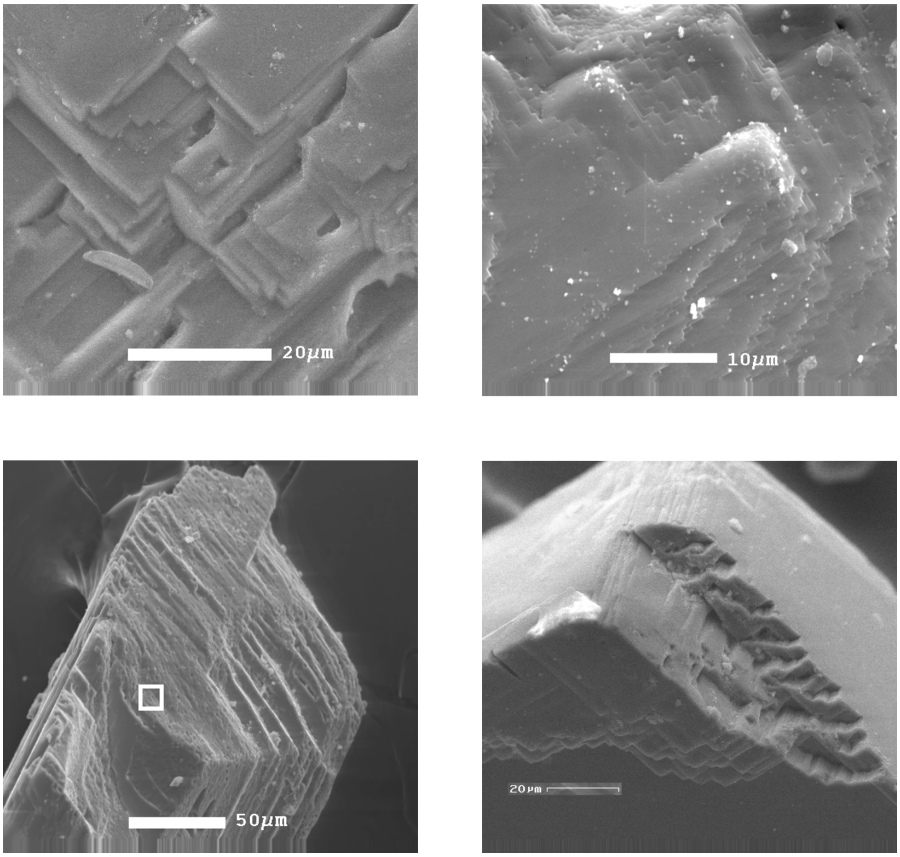

Fig. 3. Syntaxial growth of dolomite steps and terraces, run Ti10. Top Left and Top Right (scale bars 20 and 10 μm, respectively): Calcian dolomite overgrowths, with compositions ranging from 57.3 to 59.0 mole percent $CaCO_3$ based on ED spot analyses. Bottom Left: Edgewise planar growth of new dolomite. ED spot analyses within area outlined range from 52.4 to 58.7 mole percent $CaCO_3$. Scale bar 50 μm. Bottom Right: Large scale advance of lattice steps. With sufficient advance, growth would effectively heal damage inflicted by initial acid washing of seed grains. Scale bar 20 μm.

dolomite and magnesian calcite, allowing the two phases to be distinguished (fig. 5, top row).

Syntaxial overgrowth of the substrate in this run was visible as the infilling of etch pits and the formation of a bumpy, irregular surface, compositionally indistinguishable under EDS from unreacted substrate material. Dolomite heteronuclei were somewhat more calcium-rich, having between 53.2 to 58.5 percent $CaCO_3$, with some spot analyses encountering compositions slightly greater than 60 percent $CaCO_3$. Magnesian calcite compositions have an average composition from EDS of 85 percent $CaCO_3$. The alignment of magnesian calcite and dolomite rhombs suggests an underlying crystallographic control by the substrate.

Magnesian calcite.–In experiments of long duration designed to explore the influence of variations in pH (pCO_2) at fixed temperature (run Ti11, 135°C), the appearance of magnesian calcite was found to exert a strong control over the effective precipitation rate of dolomite. Figure 6 shows data collected as pH was increased in a stepwise fashion by decreasing the pCO_2 of the input solution. Although comparison of differences in total alkalinity (ΔA_T) and total divalent cations (ΔM^{2+}) indicates a good mass balance (fig. 6,

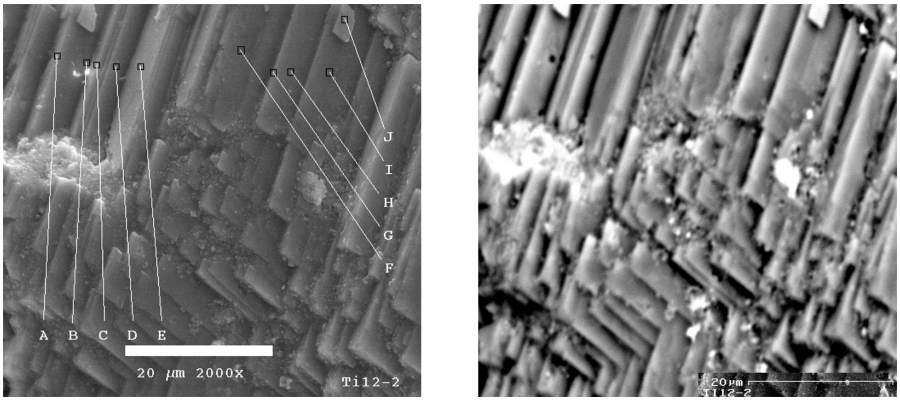

Fig. 4. Dolomite and magnesian calcite terraces, run Ti12, 150°C (scale bar 20 μm). Left: intergrowth of dolomite and magnesian calcite terraces indicated by transect of ED spot analyses (in mole percent $CaCO_3$): (A) 60.4; (B) 97.9; (C) 97.4; (D) 99.7; (E) 94.6; (F) 51.2; (G) 53.6; (H) 51.8; (I) 49.2; (J) 68.5. Right: Same field in backscattered electron mode.

top left), evaluation of the differences in calcium and magnesium uptake suggests growth of a phase more calcium-rich than the calcian dolomites typical of most runs (fig. 6, bottom left).

This is confirmed by XRD data (fig. 7, top), which indicate appearance of a magnesian calcite. Composition of this phase was determined through linear regression of structure refinement data taken from Bischoff (1985), yielding the relationship,

$$y = -363.96\,x + 1104.05,$$

in which x is the $d_{[10\bar{1}4]}$ dimension and y is the mole percent $MgCO_3$ in calcite. An apparent composition of $Mg_{0.15}Ca_{0.85}CO_3$ is calculated from the observed d-spacing of 2.992 Å. The morphology of magnesian calcite growth is shown in figure 7, bottom.

This composition is used to calculate the comparative growth rates for magnesian calcite and dolomite. Because the extent of surface area involved in each reaction is not known, we cannot calculate the absolute rate for each mineral. Despite the uncertainty regarding area, the comparison of bulk rates for calcite and dolomite still yields some insight into the competitive kinetics these two minerals. This is summarized in the bottom right panel of figure 6, which suggests that precipitation of magnesian calcite can occur at the expense of dolomite and apparently can also drive dissolution of newly formed, soluble dolomite. Calculation of saturation state revealed moderate supersaturation with respect to pure calcite (log Ω between 0.18 and 0.21).

THE EFFECT OF TEMPERATURE ON DOLOMITE PRECIPITATION RATE

In order to quantify the effect of temperature on dolomite precipitation rate, a series of experiments was run in which temperature was varied while holding the bulk composition of the input fluid (including pCO_2) constant. The reaction was allowed to proceed for a lengthy induction period (46 days at ~180°C), with the intention of allowing the reactive surface to mature and thus allow for a relatively constant surface area term throughout the experiment. Rates were then measured at 196, 186, 180, 176, and 170°C. The reactant fluid compositions, pH (25°C), and steady state precipitation

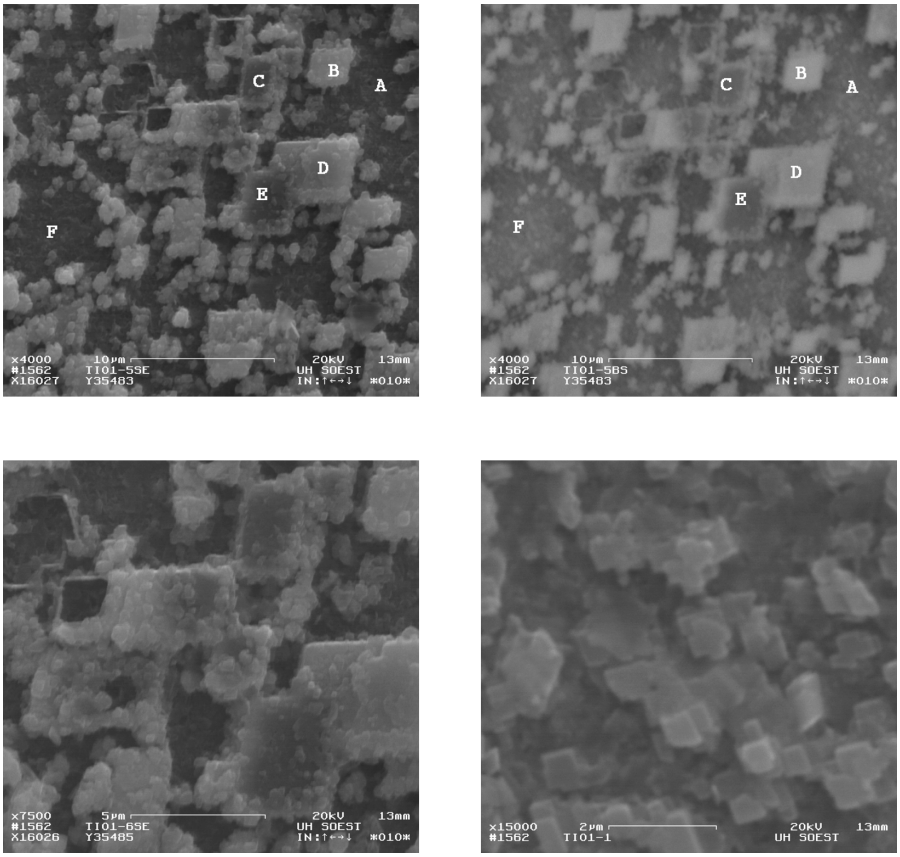

Fig. 5. Dolomite, magnesian calcite, and magnesite heteronuclei, run Ti01, 150°C, scale bar 10 µm. Top Row: Dolomite and magnesian calcite. Mole percent $CaCO_3$ from ED spot analyses: (A) 55.3; (B) 69.1; (C) 53.2; (D) 85.9; (E) 56.1; (F) 49.9. Top Left: Secondary electron image. Top Right: Backscatter image of same field. Note contrasts between dolomite (C, E, F) and magnesian calcite (D) crystals. Bottom Left: Dolomite and magnesian calcite crystal morphology, same field as in above, 5 µm scale bar. Growing crystals appear to result from agglomeration of small, poorly formed crystal nuclei, that coalesce to form a rhombic outline prior to subsequent infilling. This style of growth and the overall orientation of crystals suggests control by the underlying substrate. Bottom Right: Magnesite nucleation on dolomite substrate, scale bar 2 µm. Submicron-sized rhombs have curved and irregular crystal faces. Lack of orientation implies little control by underlying substrate lattice.

rates are presented in table 3. These data were then used to compute activation energy, according to the relation,

$$\log r = -\frac{\epsilon_A}{2.3RT} + \cdots . \tag{8}$$

The ellipsis in eq (8) encumbers terms assumed to be invariant over this span of temperature. Difficulties with this assumption are discussed below.

There is no indication that any phase other than dolomite precipitated in these runs. Solutions are undersaturated at these temperatures with respect to all carbonate mineral phases except dolomite and magnesite. The mass balances between calcium and magnesium and between alkalinity and total cations are shown in figure 8 (top row). Figure 8 (bottom left) also compares the computed stoichiometry of the newly formed solid phase with that of the observed range in natural dolomite composition. The run at

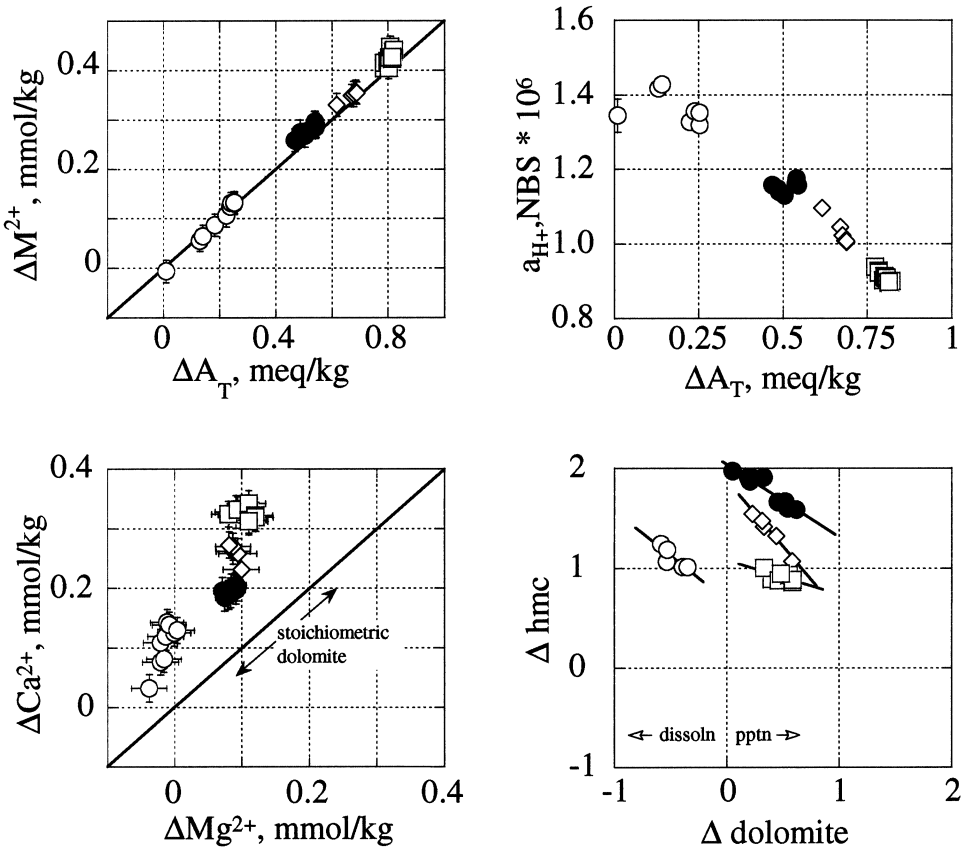

Fig. 6. Summary of results, run Ti11, 135°C. Symbols identify runs at various input pCO_2 settings. Top Left: Concentration changes (input minus output) in total alkalinity (ΔA_T) versus total divalent cations (ΔM^{2+}) show good charge balance (diagonal line is ideal relationship). Top Right: Total alkalinity (ΔA_T) decreases in linear correspondence to a_{H^+}. Bottom Left: Changes in calcium are greater than corresponding changes in magnesium, indicating formation of calcium-rich phase(s). Bottom Right: Normalized dolomite versus magnesian calcite (hmc) precipitation rates. Rates for each phase are computed using the estimated Mg content of the coprecipitated magnesian calcite (Fig. 7) and assuming a calcian dolomite (57 percent $CaCO_3$). Negative slopes (including those developed during apparent dolomite dissolution) suggest that magnesian calcite precipitation occurred at the expense of dolomite.

170°C shows an incremental uptake of calcium and magnesium; however, the total alkalinity data indicate dissolution at this temperature.[2]

X-ray powder diffraction data carefully collected from reacted seed materials indicated no phase other than dolomite present, and no shift in absolute position of the $\{10\bar{1}4\}$ peak was found in comparisons of unreacted and reacted samples. However, this result only indicates that the product phase is compositionally indistinguishable from stoichiometric dolomite. The total growth over the entire experiment was ~1 percent of the seed material. Although this extent of growth would have been sufficient to reveal any compositional differences between the seed dolomite and the new phase, it is too

[2] At 170°C, the solution is ~0.9 log units oversaturated with respect to ideal dolomite. Thus the product surface phase differs in apparent solubility by at least this much. If we make the dubious assumption that this difference in solubility is not a function of temperature, we may extrapolate it to 25°C to give an apparent ion activity product ($a_{Ca^{2+}}a_{Mg^{2+}}a^2_{CO_3^{2-}}/K_{T,dol}$), of $10^{\sim -17}$, well within the range of previous estimates (Morse and Mackenzie, 1990).

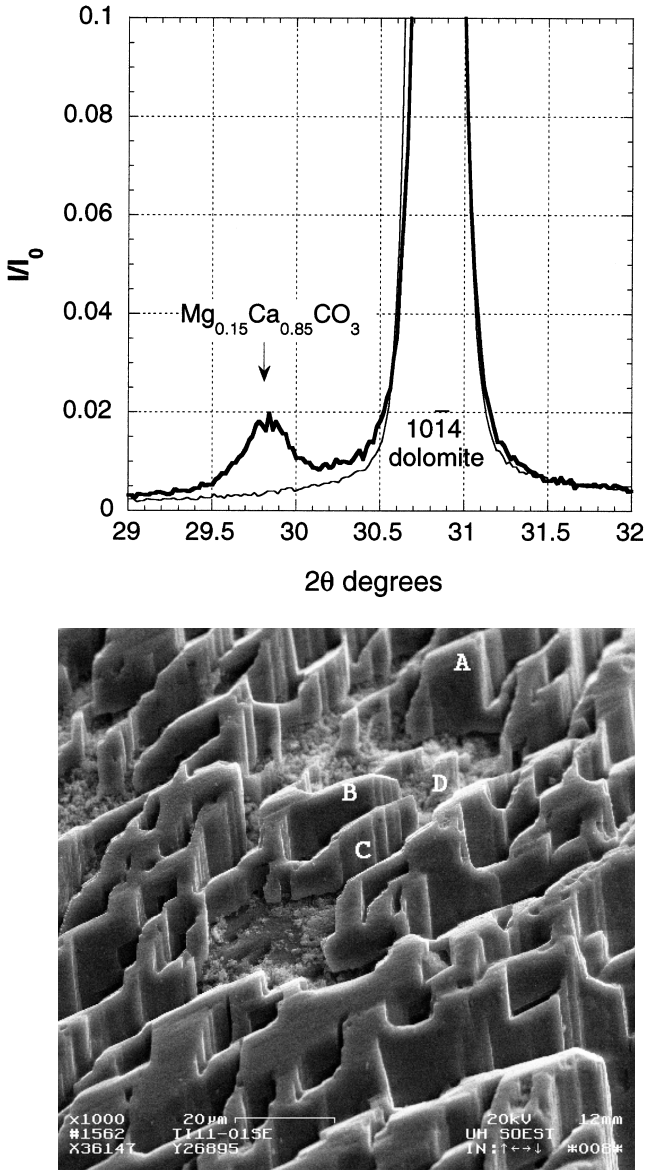

Fig. 7. X-ray diffraction and SEM data, run Ti11. Top: Detail of diffractogram shows development of magnesian calcite (heavy line), whose $\{10\bar{1}4\}$ peak position of 29.84 degrees 2Θ gives a d-spacing of 2.992 Å (peak positions are corrected to a fluorite standard). This d-spacing corresponds to the composition $Mg_{0.15}Ca_{0.85}CO_3$ using relationships computed from data of Bischoff (1985). Vertical axis is normalized intensity. Also shown for reference is unreacted seed material (light line). Bottom: SEM image of Ti11 reacted surface, scale bar 20 µm. Sites A and D are magnesian calcite (15.3 and 11.7 percent $MgCO_3$, respectively).

small to reveal any differences in cation ordering. The principal superstructure reflections ($\{10\bar{1}1\}$, $\{01\bar{1}5\}$, and $\{02\bar{2}1\}$) are of low intensity even in perfectly ordered dolomite. Thus the fact that no differences were noted either in 2Θ position or in the height or width of these peaks between reacted and unreacted samples is not conclusive. The fact

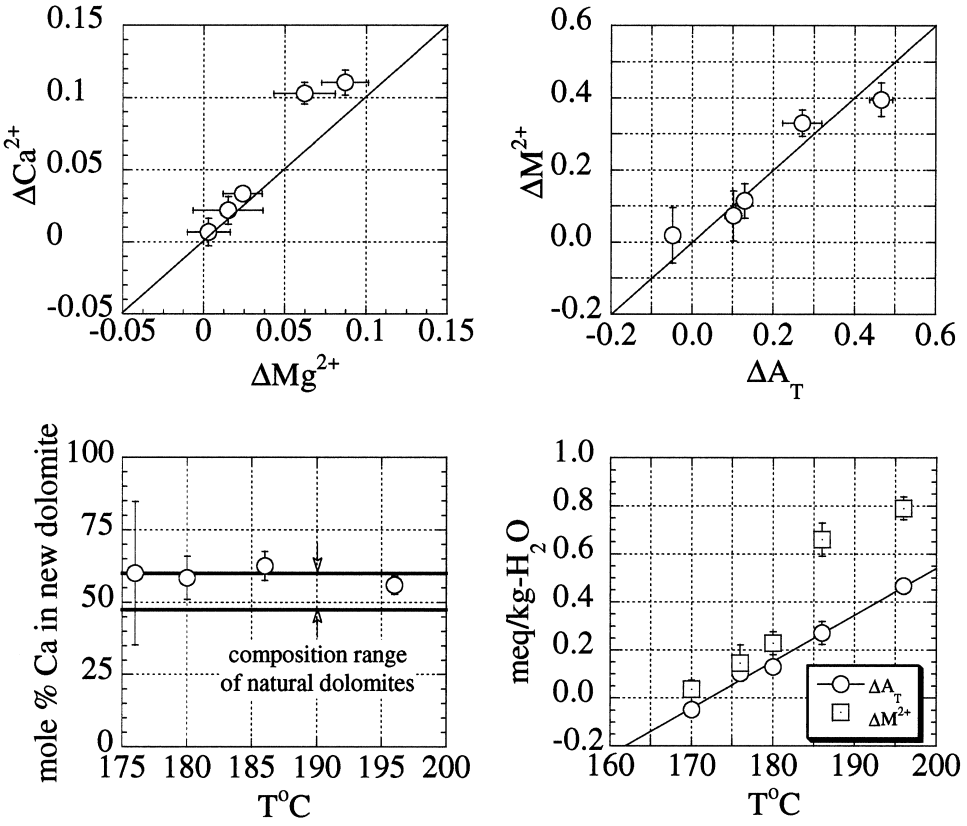

Fig. 8. Summary of results, run Ti10, 170°–196°C. Top Left: Changes in solution concentration of magnesium versus calcium due to the dolomite precipitation reaction. Ideal stoichiometry of newly formed dolomite is indicated by diagonal line, actual compositions are calcium-rich. Top Right: Changes in solution concentration with respect to total alkalinity ΔA_T versus total divalent cations ΔM^{2+}. Diagonal line indicates perfect charge balance. These values are essentially proportional to temperature, although overall balance appears to deteriorate slightly at higher temperatures. Bottom Left: Calculated mole percent calcium in newly-formed dolomite as a function of temperature. Despite increasing uncertainty with decreasing temperatures, compositions fall within the range of naturally-occurring dolomites. Bottom Right: Comparison of concentration changes with respect to temperature of total alkalinity ΔA_T and total divalent cations ΔM^{2+}. ΔA_T is linear with respect to temperature and involves smaller error.

that fluid chemistries reflect excess calcium uptake (fig. 8, top and bottom left) suggests that the new phase is at least partially disordered.

Activation energy is computed according to eq (8) by plotting the log rate versus reciprocal absolute temperature and computing a linear regression (fig. 9). The rate is represented purely as the difference between input and output concentrations, in terms of total alkalinity and divalent cations.

Uncertainties in the activation energy were approximated by computing the significance for each log rate and using this term to apply appropriate weights in a χ^2 minimization (Bevington and Robinson, 1992; Press and others, 1994). The activation energy computed from total alkalinity differences (ΔA_T) is the largest at 31.9 $\pm$ 1.6 kcal mol^{-1}. Energies using the divalent cation data yield substantially lower energies, larger uncertainties, and poorer fits and can be safely discarded on the basis that they are less than calcite (on a per mole-CO_3 basis). A summary of these regressions appears in table 4.

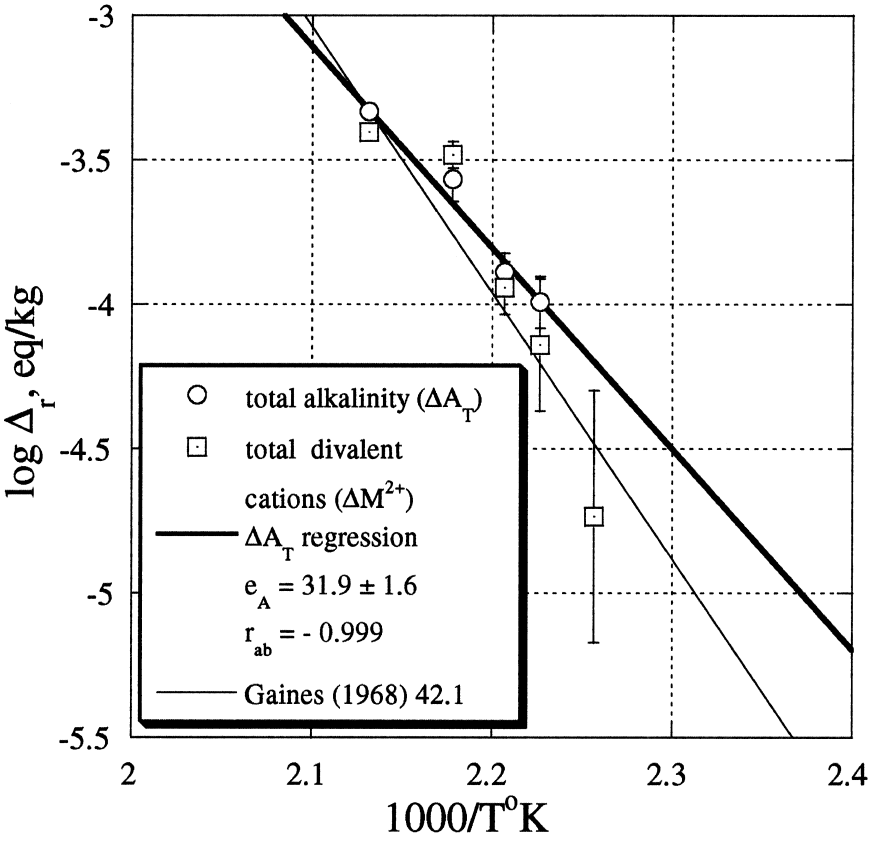

Fig. 9. Dolomite activation energy. Relationship of reciprocal absolute temperature and log of differences in total alkalinity (open circles, ΔA_T) between input and output solutions. Divalent cation data (M^{2+}, square symbols) are also shown for comparison. In addition to the principal regression computed using total alkalinity (heavy line), the slope calculated from Gaines (1968) is also shown (light line), using the 196°C point as an anchor. Activation energies in legend are in kcal mol^{-1}, and r_{ab} is the correlation coefficient of the ΔA_T fit.

Activation energy can be understood as the size of the energy barrier that reactants must surmount in order to become products. As we shall endeavor to show, dolomite precipitation is indeed a slow reaction at low temperature under most conditions (reflecting in part the size of the "frequency factor" A in eq (3). Because activation energy scales the response of the rate to changes in temperature, reactions having a large activation energy that proceed imperceptibility at low temperatures may show very significant increases in rate with relatively small increases in temperature.

Because our rate law is a function of the distance from equilibrium and not simply bulk solution composition, the assumption of temperature invariance in all righthand terms in eq (8) is not exactly true. First, the sum of the standard state chemical potentials for the dolomite precipitation reaction will change directly and indirectly as aqueous species redistribute themselves. This is shown in figure 10 by calculating the chemical potentials and activities with respect to temperature for the reaction involving basis components, using a 25°C starting composition similar to that used in these experiments. We observe that despite the decreasing availability of dissolved reactants (note the conversion of HCO_3^- and CO_3^{2-} to CO_2 with increasing temperature in fig. 10), the increasingly negative free energy of reaction to form ideal dolomite yields a region of

TABLE 4

Activation energy regressions for dolomite precipitation rate. Units of computed ϵ_A and uncertainty $\sigma_{\epsilon A}$ are kcals mol^{-1}. B is the regression intercept. ΔA_T and ΔM^{2+} refer to the difference between unreacted input and reacted output solutions, in equivalents and moles of total alkalinity and total divalent cations, respectively, per kilogram-solution.

T°C	1000/T°K	$\log \Delta A_T$	$\sigma_{\log \Delta A_T}$	$\log \Delta M^{2+}$	$\sigma_{\log \Delta M^{2+}}$
196	2.1315	-3.3324	0.0132	-3.4032	0.0127
186	2.1779	-3.5667	0.0385	-3.4819	0.0228
180	2.2068	-3.8884	0.0327	-3.9427	0.0454
176	2.2264	-3.9923	0.0446	-4.1394	0.1147
170	2.2566			-4.7336	0.2183

source	ϵ_A	σ_{ϵ_A}	B	σ_B
ΔA_T	31.86	1.57	11.51	0.74
ΔM^{2+}	21.93	1.90	6.83	0.89
ΔM^{2+}*	20.51	1.94	6.17	0.91

*Excluding 170°C datum .

favorable reaction at temperatures $\gtrsim$150°C. However, the assumption above is only reasonable if $n\Delta_r\mu$ (or its temperature derivative) is small compared to ϵ_A over the span of experimental temperatures.

Second, we have made the assumption that it is the distance from equilibrium with respect to ideal dolomite and not a phase rendered more soluble by calcium enrichment and cation disordering that drives this reaction. Changes in cation ordering with temperature, so characteristic of dolomite crystal chemistry (Goldsmith, 1983; Morse and Mackenzie, 1990), are indeed probably a feature of the dolomite phase forming in

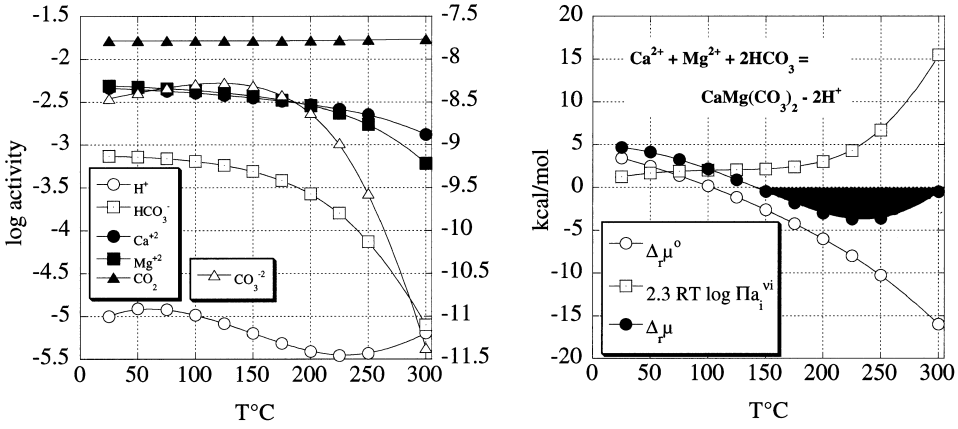

Fig. 10. Dolomite precipitation reaction from basis components. Left: Activities of dissolved species from equilibrium model. These are computed with respect to temperature, using a pH (25°C) of 5.00 and a starting composition (in moles per kg-H_2O) of [$CaCl_2$] = [$MgCl_2$] = 0.01 and [$NaHCO_3$] = 0.001. Note the complex behavior of pH. Decreasing activities of free calcium and magnesium with temperature correspond to increasing association with carbonate and bicarbonate. Carbonate ion activity refers to righthand scale. Right: Chemical potential for reaction to form ideal dolomite from basis components, using the starting composition shown in left frame. Shaded region of dolomite supersaturation is a function largely of its decreasing solubility with respect to temperature.

these experiments. The use of ideal dolomite in Ω calculations is necessitated by the overall uncertainty in dolomite's solubility and the positive free energy contributions of cation disordering and excess calcium. Third, because of the high ratio of solid surface area to solution, changes in reaction rate also have an effect on solution chemistry. Increases in the rate by virtue of temperature also brought about increased consumption of reactants, which in turn served to depress the ion activity product and in turn probably depressed the rate. As a result, steady state saturation indices actually decreased with increasing temperature. Had the reactor been capable of maintaining a truly constant saturation index independent of temperature and reaction rate, measured rates at the higher temperatures would most likely have been higher still, giving a greater slope in figure 9, and thus a higher computed activation energy. Thus the calculated value of 31.9 kcal mol^{-1} most likely represents a minimum value.

Last, changes in the dominant reaction mechanism with temperature may give rise to corresponding changes in activation energy, visible as changes in slope in figure 9. These uncertainties clearly endow the derived parameters in the rate equation with nontrivial errors that are difficult to quantify. Subsequent work, particularly in the form of detailed solubility measurements as a function of temperature and solid phase composition, may no doubt reveal more complex governing relationships at work than those implicit in this simple treatment.

The value of 31.9 kcal mol^{-1} is also lower than the value of 42.1 kcal mol^{-1} obtained from an analysis of unpublished data from Gaines (1968, rates computed from 220° 250°C; see also Arvidson and Mackenzie, 1997) which in turn is lower still than the only published value of 49 kcal mol^{-1}, determined from rates at temperatures from 252° to 295°C by Katz and Matthews (1977).[3] This begs the question, how is activation energy dependent on the properties of the newly forming dolomite phase?

Answers to this question must be somewhat speculative in nature given the precision, temperature range, and small number of data. Furthermore it is not possible to calculate satisfactorily an error estimate for either of the other two numbers, which is necessary given the sensitivity of the slope $-\epsilon_A/R$ to errors in rate measurement (fig. 9 and table 4). It is conceivable that the differences in apparent activation energy arise from the differences in experimental regimes. For example, in the experiments of Gaines (1968) and Katz and Matthews (1977), growth of dolomite took place in brines with a very large excess of $CaCl_2$-$MgCl_2$ over dissolved carbon, whose only source is dissolution of $CaCO_3$ reactant.

More likely, however, the discrepancies in energy reflect differences in the composition and cation ordering of the dolomite phase. The increasing error in the apparent stoichiometry with decreasing temperature (fig. 8, bottom left) makes it difficult to discern any significant changes in stoichiometry with temperature from our data. However, based on fluid chemistry data alone, the phases produced also tend to be richer in calcium compared with those produced in earlier published experiments at higher temperatures. For example, all end phase dolomites produced from 252° to 295°C in Katz and Matthews (1997) are essentially stoichiometric, with only $\sim \pm 1$ percent excess calcium or magnesium. The stoichiometry of recrystallized dolomite also tends to improve with increasing temperature, and the composition of first-formed dolomite phases at any temperature tends to be richer in calcium compared to subsequent phases (50°-200°C, Malone, Baker, and Burns, 1996). Gaines (1968) also observed an increase in $MgCO_3$ with increasing temperature (220°-250°C), although the same effect in his experiments could be observed at fixed temperature (200 and 220°C) as the ratio of magnesium to calcium in solution was increased from 0.5 to 1.0 (his table 2, p. 30). It is thus possible that the lower activation energy observed reflects a reduced energy barrier to forming calcian dolomities.

[3] Activation energies computed from their data range from 46 to 50 kcal mol^{-1}

The reduction in activation energy with increase in excess calcium content must be ultimately related to the differences in energy requirements of dehydrating calcium versus magnesium ion prior to incorporation within the growing dolomite lattice. The importance of magnesium on dehydration has been considered in detail by Lippmann (1973), and is also relevant in terms of the link between dolomite and evaporitic environments, where water activity is potentially minimized. This can be illustrated by comparing magnesite with calcite. Lippmann (1973), using hydration enthalpy data from Noyes (1962) and a model for the electrostatic energy of the ion-dipole bond as a function of ionic radius and dipole moment, estimated the activation energy for magnesite growth to be 12.8 kcal mol^{-1} greater than that for calcite. Both minerals have similar solubilities ($10^{-8.48}$ versus $\sim 10^{-8.04}$), and they are structural isotypes. If we assume that the mechanism of growth is identical in both minerals (and thus that the values for frequency factor and reaction order are identical), then the log ratio of their rates is proportional to the differences in activation energies (compare p. 82, Lippmann, 1973),

$$\log \frac{r_{cal}}{r_{mag}} = \frac{\Delta \epsilon_A}{2.303RT}$$

In equivalently supersaturated solutions, this number is ~10 at 25°C. This very large difference in estimated rates is reflected in the distribution of magnesite in modern surface environments, whose scarcity rivals that of dolomite. If dolomite growth is viewed as a process of constructing alternating layers of calcite and magnesite, then the rate of dolomite growth may be essentially limited by that of the "magnesite" layer. If, at a given temperature, dehydration of calcium requires less energy than magnesium, calcium may become incorporated in its stead in spite of its overall destabilizing influence on the bulk solid. The greater ease of calcium versus magnesium incorporation at this step is thus reflected in a reduction in activation energy for the dolomite crystal.

Lippmann (1973) has carried this model somewhat further in postulating that it is the influence of "activated" carbonate ions that accelerate the rate of magnesite growth. These anions, by virtue of greater translational or vibrational energy, can displace water dipoles bonded to surface cations. Carbonate anions, because of their larger size, are less completely hydrated and thus can attract more cations and start the process anew. In this sense, carbonate anions compete for surface cations with water dipoles. With respect to dolomite growth, this model draws some support from the fact that much of the increase in saturation index for data used to constrain the rate law of Arvidson and Mackenzie (1997) comes about from carbonate ion activity.

If the rate of dolomite growth is fundamentally limited by the incorporation of magnesium in the $MgCO_3$ layer, then one would expect its activation energy to be related to those of the magnesium-bearing single carbonates. This expectation is also anticipated by the essentially linear relationship between excess calcium and enthalpy observed by Chai, Navrotsky, and Reeder (1995). The activation energy for calcite is relatively well known, and we have used the value of 9.4 ± 0.9 kcal mol^{-1} from Kazmierczak, Tomson, and Nancollas (1982). Using the difference of 12.8 kcal mol^{-1} computed by Lippmann (1973) yields a theoretical value of 22.2 kcal mol^{-1} for magnesite. To portray the activation energy for all phases on the same scale, we must divide dolomite's activation energy in half to give units of kilocalories per mole of single carbonate, $Ca_{1-x}Mg_xCO_3$. The results are shown in figure 11.

It is apparent that the activation energy observed for the dolomite phase formed in this experiment is slightly higher than that predicted by assuming magnesium dehydration to be the controlling step. This difference probably reflects the energy of (partial) ordering. Comparison with the energy calculated for relatively well-ordered dolomites synthesized by Gaines (1968) shows an increase of ~11 kcal mol^{-1} over the linear value. This activation energy associated with the ordering reaction is in at least qualitative

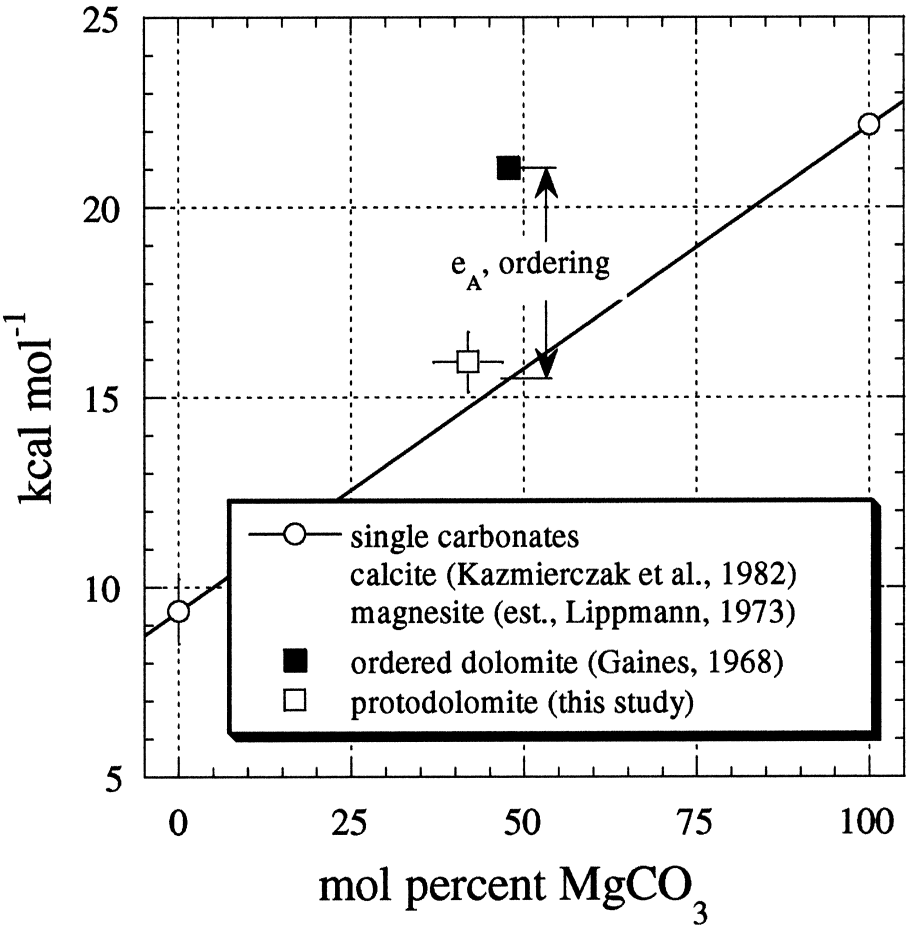

Fig. 11. Relationship of activation energy to dolomite composition. A linear relationship is assumed for the change in activation energy with $MgCO_3$, using energies for calcite (Kazmierczak, Tomson, and Nancollas, 1982) and magnesite (computed from Lippmann, 1973). Despite the extent of calcium enrichment in dolomites synthesized in this work, their activation energy is only slightly in excess of that predicted for magnesium dehydration only: this implies some activation energy involved in cation ordering. This compares favorably with data computed from Gaines (1968), in which relatively well-ordered phases were formed. If ordering in the latter case is assumed to be essentially perfect, the activation energy involved in ordering is calculated to be ~11 kcal (per mole of $CaMg(CO_3)_2$).

agreement with values ranging from 8 to 11 kcal mol^{-1} computed using data from Malone, Baker, and Burns (1996) for the rate of recrystallization of disordered Ca-Mg carbonate starting materials to ordered phases over the temperature range 98° to 197°C.

GENERAL RATE LAW FOR DOLOMITE PRECIPITATION

We may now combine these rate data with those available from the literature. These "literature" values are discussed in Arvidson and Mackenzie (1997; see also Arvidson, 1998) and remain unchanged except that saturation states were recalculated using our aqueous model for consistency.[4] The dataset in its entirety appears in table 5.

[4] Previous saturation indices in Arvidson and Mackenzie (1997) were computed using SOLMINEQ.88 (Kharaka and others, 1988) and EQ3NR (Wolery, 1992).

TABLE 5

Dolomite saturation indices of experimentally reacted solutions. The entry for logr + ϵ_A/2.3 RT assumes an activation energy value of 31.9 kcal mol^{-1} computed from run Ti10. Rates (r) have units of mols cm^{-2} s^{-1}. Entries 1 through 9 are described in Arvidson and Mackenzie (1997) and appear here with recomputed saturation states. Surface area was estimated by geometric means ("sem") or by BET method where indicated.

no.	source/run	T°C	$\log \Omega_{dol}$	$\log r + \frac{\epsilon_A}{2.3\ RT}$	surface area
1	km77-263	263	0.8804	3.268	
2	km77-252	252	0.8837	3.243	
3	ga68-250	250	1.1521	4.672	
4	ga68-240	240	1.1532	4.686	
5	ga68-230	230	1.1565	4.532	
6	ga68-220(1)	220	1.1610	4.436	
7	ga68-220(2)	220	1.3073	5.112	
8	ga68-220(3)	220	1.4157	5.305	
9	si90-218	218	1.463	4.951	
10	ss08-115	115	2.5165	6.964	sem
11	ti01	150	1.9702	5.934	"
12	ti02	150	1.5985	4.790	"
13	ti05	150	1.4605	4.446	"
14	ti08	150	0.7268	3.667	bet
15	ti09	150	0.5479	3.781	"
16	ti10-196	196	0.5084	2.537	"
17	ti10-186	186	0.5939	2.619	"
18	ti10-180	180	0.7748	2.508	"
19	ti10-176	176	0.6761	2.555	"

Values for the parameters n and log A are obtained by computing a regression for these data according to the original expression in Arvidson and Mackenzie (1997):

$$\log r = -\frac{\epsilon_A}{2.3\ RT} + \log A + n \log (\Omega - 1). \quad (3)$$

The value for activation energy computed earlier (31.9 kcal mol^{-1}) is used. It should be noted that data judged to be of poor quality, either because of problems with the reactor itself or because of uncertainties regarding the effect of coprecipitating phases, were excluded from this treatment. The one exception is the inclusion of data from run Ti01, in which magnesite and magnesian calcite were also found. These phases, developed as heteronuclei on the surface of the dolomite substrate, should have had the effect of reducing the surface available for dolomite growth. Therefore the rate appearing in table 5 probably represents a minimum value, because it was computed by assigning the total surface area to dolomite precipitation. The reason for including this datum is to exert as much constraint as possible on the high saturation end of the curve.

Errors for all rates (except those computed from published hydrothermal bomb experiments) have been estimated by combining the titration errors with the uncertainty in the activation energy value using standard propagation of error. No provision is made for errors in saturation state calculations. Surface area data from BET analysis are used where available. BET areas were generally higher than geometric areas for reacted samples from runs Ti08, Ti09, and Ti10. SEM images of these samples also showed large enhancements of surface area through development of growth features. Although mixing of geometric and BET estimates may not be altogether prudent, this did provide a means of reconciling the visible differences in surface area among samples that simple geometric estimates do not provide.

The regression results appear in figure 12. Inclusion of data only from early, high supersaturation experiments using geometric area estimates results in an overall reaction order of 2.26 and frequency factor log A of 1.05. Regression of all data (including those derived from the literature) causes the order to diminish to 1.88 but increases the log frequency term by more than an order of magnitude to 2.09.

Our rate expression is a nonlinear function of its parameters, activation energy, and order. The values obtained by regression for these parameters are sensitive to errors in the observables (rates and saturation indices), and the computed model rate will thus also be sensitive to the parameter values chosen from the regression analysis. These depen-

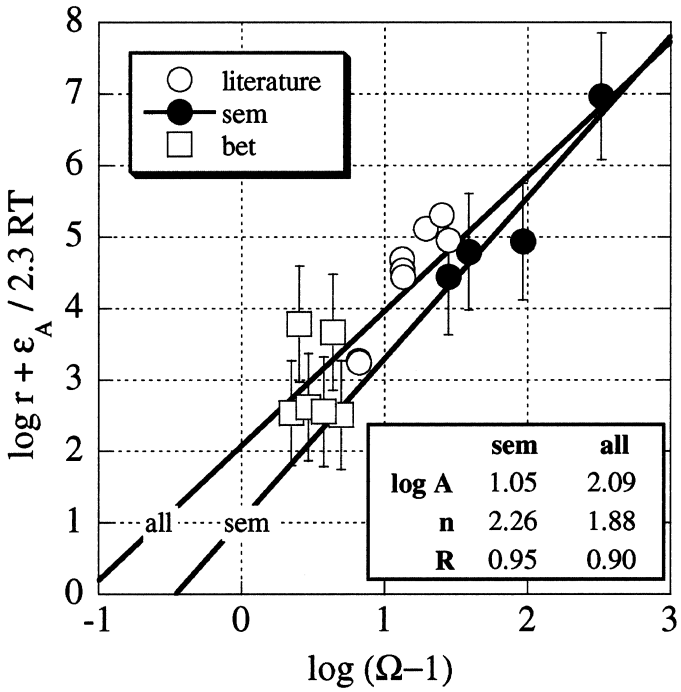

Fig. 12. Dolomite reaction order (n) and frequency factor (log A). These parameters are computed through regression of existing dataset and appear together with the correlation coefficient (R) in the box in the lower righthand corner. Open circle symbols refer to literature data, described in Arvidson and Mackenzie (1997), closed circles to experiments conducted at higher supersaturations in which surface area was estimated from SEM images (sem), and open square symbols to experiments at lower supersaturations and generally higher temperatures where surface area was measured by BET analysis (bet). Regressions are computed using both the high supersaturation data alone (sem) and all data (all). Both lines assume an activation energy of 31.9 kcal mol^{-1}.

dencies are also not separable, that is, selection of a new parameter value, for example activation energy, necessarily changes the fitted values of order and frequency. These interactions are explored further by computing model fits using different values for activation energy. In figure 13, orders, frequencies, and the resulting 25°C rate constants have been computed using a span of activation energies: 25, 31.9, 42.1, and 48 kcal mol^{-1}. The latter two values are taken from the analysis of data from Gaines (1968, see also Arvidson and Mackenzie, 1997) and published values from Katz and Matthews (1977), respectively. The strong sensitivity of the model rate is clearly shown through the change in the rate constant extrapolated to 25°C, which varies inversely by ~0.3 log units per kcal of activation energy. Thus as the temperature dependence of the rate (measured at high temperatures) increases, the extrapolated value of the rate at earth surface temperatures decreases dramatically.

The relationships expressed in figure 12 do confirm our original working hypothesis (Arvidson and Mackenzie, 1997) that dolomite precipitation rate is a positive function of the distance from equilibrium. At this point it is difficult to evaluate whether the apparent scatter in the data reflect (in addition to uncertainties in surface area) differences in composition (and thus cation ordering) of the phase under reaction. The enthalpy data of Chai, Navrotsky, and Reeder (1995) suggests that solubility is a very strong function of the extent of calcium substitution. Thus the "distance" from equilibrium of the phase undergoing precipitation should vary according to its composition. Spot EDS analyses of what is clearly new dolomite to run Ti10 (170°-196°C, fig. 3) do show it to be calcium-rich in composition, in agreement with the fluid chemistry data. The variation in these EDS analyses also suggests variability in the surface composition, and although part of this variability may be an artifact of the instrument's semi-quantitative resolution, the data were nonetheless fairly reproducible. No significant differences were found between reacted and unreacted seed materials in the position or contour of the $\{10\bar{1}4\}$ diffraction peak. However, this may simply reflect the difficulty of resolving phases insufficiently different in composition. At this point, it seems safest to conclude that the dolomite phase is probably variable in composition, and that this variation may affect the rate as well.

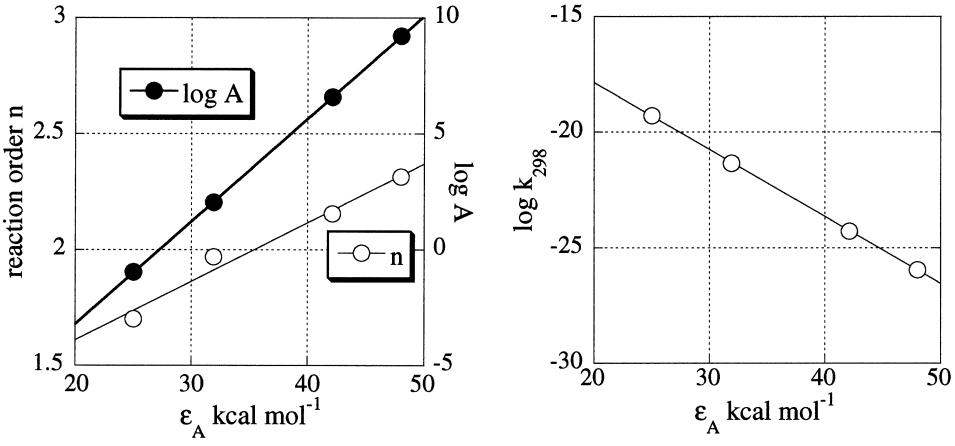

Fig. 13. Model rate law sensitivity to variation in activation energy. The total dataset was fit using different ϵ_A estimates: 25, 31.9, 42.1, and 48 kcal mol^{-1}. Left: Change in order and frequency factor. Right: The overall rate constant at 25°C shows a dependence of ~0.3 log units per kcal.

RELEVANCE OF EXPERIMENTAL RESULTS TO NATURAL CARBONATE MINERALS

One of the key issues to resolve in the dolomite problem is the relevance of experimental data collected at temperatures far in excess of surface environments. Given the extrapolated rates of dolomite precipitation at 25°C or lower, it is doubtful that any experiments conducted at these temperatures, outside those capable of atomic scale resolution, will be able to observe dolomite formation directly on laboratory time scales. To illustrate this point, the time required to precipitate sufficient dolomite to give 10 percent of the original mass of seed material has been calculated, given the following starting conditions: 0.001 m $NaHCO_3$, 0.01 m $MgCl_2$, and sufficient $CaCO_3$ dissolved to given saturation with respect to calcite as we increase temperature. Figure 14 shows the results of these calculations. In a closed system, the rate law in its current form predicted that hundreds of years of laboratory observation would be required to detect this extent of reaction. In a 0.5 m matrix of NaCl, decrease in activity coefficients and increased complexation retard the rate further. The time required shortens considerably if the starting concentration of $MgCl_2$ is increased to 0.05 m; however, tens of years are still required at 25°C.

The case studies of natural dolomite precipitation presented in Arvidson and Mackenzie (1997) support the observation that dolomite currently forming in low temperature environments responds strongly to increases in carbonate alkalinity, supplied either by aragonite dissolution or bicarbonate production during sulfate reduction.

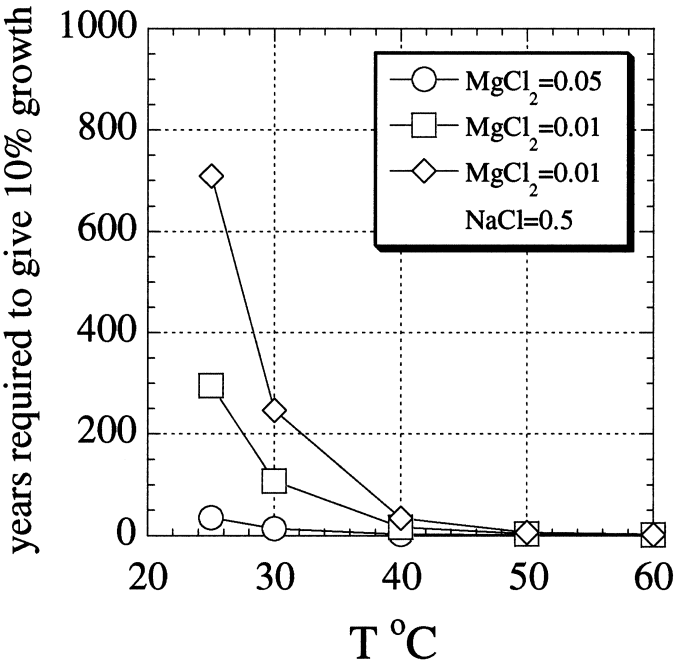

Fig. 14. Model reaction times for low temperature dolomite growth. The time required to precipitate sufficient dolomite on a fixed substrate surface area to yield 10 percent increase in mass relative to the substrate is estimated as a function of temperature. Three different curves are calculated, all containing 0.001 m $NaHCO_3$ and sufficient dissolved $CaCO_3$ to bring about calcite saturation: 0.01 m $MgCl_2$, 0.01 m $MgCl_2$ in a 0.5 m NaCl matrix, and 0.05 m $MgCl_2$. The times estimated for 25°C reactions (10^1 to 10^2 yrs) suggest that direct laboratory observation under these conditions is infeasible. Note however, that the time required for reaction at ~50°C, although still lengthy, are not unreasonable, in qualitative agreement with the results of Malone, Baker, and Burns (1996).

This effect is at least partly borne out by these data, in which the log rate[5] is a strong function of saturation index, which in turn mostly reflects the change in carbonate ion availability. These data (with few exceptions) reflect a more or less constant ratio of calcium to magnesium and thus are inadequate to evaluate how the rate may be influenced by changes in cation ratio, or by other influences such as ionic strength (although the use of activities versus concentrations in the rate expression to some extent accommodates this term).

The overall relevance of experimental kinetic data for the dolomite problem also depends on whether one can point to features common to other carbonate phases formed in both natural and laboratory systems. Two important observations can be made:

1. *Significance of growth textures.*–Although the data are insufficient to establish a quantitative relationship, the growth features observed appear to be a function of the extent of supersaturation. Growth at lower degrees of supersaturation occurs as layers in apparent syntaxial continuity with the original grain surface. These layers closely resemble those developed in published calcite growth kinetics experiments (compare figs. 3 and 4 with 9, Shiraki and Brantley, 1995) and imply a mechanism of polynuclear growth, in which the surfaces accrete through the growth, spread, and coalescence of multiple nucleation points.

At high supersaturations, in addition to what may be secondary nuclei forming on the seed surface, larger rhombic crystals form via the aggregation of submicro-sized nuclei. Figure 5 clearly shows newly forming "skeletal" crystals whose orientation bears an obvious crystallographic relationship to the underlying substrate seed material. This style of growth, in which larger crystals form as aggregates of small nuclei, appears quite similar to that described by Carballo, Land, and Miser (1987) in supratidal dolomite forming in contact with little-modified seawater (compare fig. 9, p. 158, Carballo, Land, and Miser, 1987).

These observations are significant for two reasons. First, they imply a certain continuity with calcite in terms of the overall mechanics of crystal growth at low relative supersaturation. Thus it is likely that the transitions in mechanism predicted from classical nucleation and crystal growth theory (for example, growth via screw dislocation, growth rate proportional to defect density), perhaps not surprisingly, can also be applied to dolomite, assuming that sufficient measurements are feasible.

Second, the fact that syntaxial growth could be sustained at low overall saturation index, often with little or no "induction period," is relevant to the growth of both synthetic and natural dolomite. Previous experimental work has focused almost exclusively on the conversion of calcite to dolomite (that is, "recrystallization"). The difficulty in forming dolomite at sedimentary temperatures in this type of experiment is a large part of the original dolomite problem (Arvidson, 1998). However, the overall reaction in this case involves the removal of available mineral substrate, through dissolution of reactant $CaCO_3$. This dissolution thus acts to remove surface area that would otherwise offer potential growth sites. In contrast, the data presented in this work imply that syntaxial growth on existing surfaces can be sustained at low supersaturations, whereas formation of discrete heteronuclei as seen in figure 5 requires significantly higher supersaturation.

2. *Significance of other coprecipitating carbonate phases.*–Other phases, including magnesite and magnesian calcite, also formed, often as intergrowths in intimate contact with new dolomite surfaces. Magnesian calcite formed at very low (pure calcite) supersaturation. However, there is no indication, either from reacted fluid history of surface analysis, that magnesian calcite acts as any kind of precursor to dolomite growth in these

[5] By using the term $\log r + \epsilon_A/RT$, the intention is to compare rates that are essentially normalized with respect to temperature and thus primarily observe the effect of changing saturation state.

experiments. This observation is direct contrast to earlier synthesis work, discussed in Arvidson and Mackenzie (1997), in which dolomite is formed through reaction of $CaCO_3$ and $(Ca,Mg)Cl_2$ solutions. The appearance of magnesian calcite in these earlier experiments has been cited elsewhere (for example, Katz and Matthews, 1977) as evidence that it plays a role as a reactive intermediate.

No evidence of this relationship was found. On the contrary, the nucleation and growth of calcite typically arrested or at least severely diminished the rate of dolomite precipitation. In fact, much of the challenge of our experiments conducted at high supersaturations was to promote dolomite precipitation without the advent of calcite nucleation and growth. The relationship between dolomite and calcite is thus more accurately described as competitive, and is consistent with the relationship observed by Wenk and Meisheng (1993) at Abu Dhabi, in which aragonite, magnesian calcite, and (proto)dolomite are observed as an intimate mixture of phases that nonetheless do not necessarily form a reaction series.

The observation that dolomite competes poorly with metastable magnesian calcite, at least under the conditions of these experiments, implies that rather specific conditions must persist in order for dolomite to dominate in terms of mineral distributions. The growth of sedimentary dolomite under conditions of greatly elevated alkalinity concentrations, for example by way of sulfate reduction, thus may not be purely a matter of grossly elevated supersaturations and implies additional dependencies, perhaps on the ratio of Mg^{2+} to Ca^{2+} activity, not explicitly described by the rate law in its current form.

Are the dolomite overgrowths formed in these experiments simply calcium-rich, disordered synthetic phases having little relevance to mineral formation at earth surface temperatures? They are not simply magnesian calcites—~15 mol percent magnesian calcite did form but is identifiable from XRD and SEM data as a distinct, although clearly metastable, phase. The activation energy of this calcite phase, based on figure 11, would be <12 kcal mol^{-1}. It is indeed likely that both the cation disorder and solubility of the surface dolomite phase of these experiments are higher than the underlying substrate—this is suggested both by the theoretical calculation of activation energy from magnesium ion dehydration enthalpies (fig. 11), and the 170°C dissolution of previously formed material despite calculated supersaturation with respect to ideal dolomite (run Ti10). However, poor cation ordering and excess calcium are hallmarks of Holocene dolomite as well, as discussed in Arvidson (1998). In addition, the initial precipitate in many sedimentary minerals is typically imperfect with respect to order and contaminants: the magnesian calcites themselves are excellent examples, containing excess water, sodium, sulfate, and bicarbonate, and surface defects, in addition to anion positional disorder introduced by magnesium substitution (Busenberg and Plummer, 1986; Mackenzie and others, 1983; Morse and Mackenzie, 1990). These positive contributions to free energy are lost during subsequent episodes of recrystallization during diagenesis, resulting in the formation of a stable, low-magnesium calcite. The question is whether first-formed protodolomites react along similar stabilization pathways and are thus precursors to the stoichiometric, well-ordered phases typical of Paleozoic sequences.

In summary, experiments designed to measure dolomite precipitation rate over a range of temperature and solution composition have yielded model parameters for a reaction rate law having a simple dependence on saturation index. Precipitation rates measured at 196°/176°C give an activation energy for the overall precipitation reaction of 31.9 ± 1.6 kcal mol^{-1}. This value is ~10 kcal mol^{-1} less than the estimate obtained from Gaines (1968). Comparison of these energies with those estimated from a comparison of hydration enthalpies of Ca^{2+} versus Mg^{2+} suggests that Mg^{2+} dehydration is a major component of activation energy, with the remaining energy involved in cation ordering. Selective fitting of rate data yields an overall reaction order of 2.26 and a pre-exponential frequency term of 1.05 (log_{10} units). This yields a rate constant at 25°C of

$10^{-22.3}$. As in any empirical kinetic model, the values of these parameters are model-dependent. The combination of high activation energy and relatively high order yield a reaction that is strongly sensitive to changes in both temperature and saturation state. Extrapolations to laboratory conditions suggest infeasibly long reaction times at 25°, but with significant improvement at slightly higher temperatures.

Growth textures observed in these experiments suggest syntaxial growth through aggradation of existing steps dominates at lower supersaturations, with evidence of distinct heteronuclei only observed at supersaturations of $\log (\Omega - 1) \gtrsim 2$. In the latter case, growth appears to proceed by the agglomeration of small nuclei to form larger crystals. The growth of magnesian calcites ($\sim$15 mole percent $MgCO_3$) where observed appears to outcompete dolomite for available dissolved components, and thus largely buffers dolomite precipitation subsequent to its appearance.

CONCLUSIONS

The principal results can be summarized as follows:

1. The rate of dolomite precipitation, measured in a steady-state dolomite-seeded reflux reactor over a range of temperatures at fixed bulk composition and at variable composition and temperature, is shown to be a strong function of temperature and solution composition. Influence of the solution composition is treated by inclusion of an estimate of the saturation index (Ω) relative to ideal, ordered dolomite. Influence of temperature is described by a classical Arrhenius-type formulation, resulting in an overall simple expression of the rate:

$$r = Ae^{-(\epsilon_A/RT)} (\Omega - 1)^n.$$

Selective fitting of rate data gives values for activation energy (ϵ_A), pre-exponential frequency factor (A), and reaction order (n) of 31.9 kcal mol^{-1}, $10^{1.05}$, and 2.26, respectively. The value for activation energy can be compared with those computed from other sources and with those estimated through consideration of heats of cation hydration. This comparison suggests that Mg^{2+} dehydration represents a significant component of ϵ_A; an activation energy associated with cation ordering was estimated at $\sim$10 kcal mol^{-1}.

The composition of the dolomite forming in these experiments calculated from solution mass balance and EDS spectroscopy of growth surfaces is calcium-rich, with values typically between 55 and 58 mol percent $CaCO_3$. Based on these compositions, comparison of activation energy, and evidence of dissolution in certain runs, the dolomite forming in these experiments is most likely protodolomite, sensu Graf and Goldsmith (1956), with a solubility greater than that of the underlying dolomite substrate.

2. Growth textures observed in these experiments resemble those in published experiments for calcite precipitation on seed crystals. The style of growth varies according to the extent of supersaturation, with lower supersaturation promoting simple migration of surface steps and kinks. Higher supersaturations are associated with the development of complex nucleation centers consisting of submicron-sized nuclei. These particles appear to accrete in patterns apparently controlled by the crystallography of the underlying substrate. These textures also resemble those observed in low temperature natural dolomites developing in supratidal sediments in contact with pore fluids of near-marine composition.

3. The effective dolomite precipitation rate is maximized when there is no competition from other carbonate phases, in this case principally magnesian calcite. Calcite appears to nucleate rapidly given even slight oversaturation, and those experiments in which growth of both phases could be monitored showed calcite to form essentially at the expense of coprecipitating dolomite. SEM/EDS analysis of growth textures show

fine-scale intergrowths of calcite and dolomite layers in apparent crystallographic continuity, raising the possibility that such developments are twins with shared axes. Magnesite was also observed at bulk magnesium to calcium ratios similar to seawater, forming small, subhedral rhombic crystals. In contrast with the common perception, no evidence could be found that magnesian calcite acts as a reactive intermediate. Although the approach to a steady state reaction was variable in duration and direction, no distinct trends could be found in terms of evolution in composition of the newly precipitating solid.

The strong dependence on temperature and saturation state observed in these experiments suggests that it is the overall low rate of dolomite precipitation relative to competing carbonate phases at surface temperatures that determines dolomite's abundance in a sedimentary regime. Consideration of the relationship between dolomite and calcite in terms of activation energies also suggests, however, that small increases in temperature would yield significant increases in dolomite precipitation rate relative to calcite, particularly in cases where calcite is either minimally supersaturated or undersaturated.

Solving the dolomite problem demands resolving the discrepancy between modern and ancient abundances of dolomite. Modern apparent fluxes of magnesium to the dolomite "reservoir" are very small, and seawater exchange cycling at mid-ocean ridges currently serves as the primary Mg sink. However, if the abundance of dolomite reflects its absolute precipitation rate in the environment, the high sensitivity of the rate to changes in temperature and seawater chemistry raises the possibility that past environmental shifts have altered the fluxes of magnesium to carbonate versus basalt reservoirs. Although the control and history of seawater composition has long been of interest, recent work tends to be largely dismissive of the importance of dolomite (Hardie, 1996; Stanley and Hardie, 1998). These relationships will be explored in a companion paper.

ACKNOWLEDGMENTS

Acknowledgment is made to the donors of The Petroleum Research Fund, administered by the American Chemical Society, for support of this research while RSA was at the University of Hawaii. RSA wishes to thank Miriam Bertram for her kind assistance with SEM work; assistance with experimental work was also provided by Michael Guidry, L. May Ver, Terri Rust, and Joseph Resing. The authors also wish to thank Jack Middelburg, Lee Kump, James Dockal, and an anonymous reviewer for their thoughtful criticism of an earlier drafts of this paper. School of Ocean and Earth Science and Technology Contribution No. 4806.

REFERENCES

Alderman, A. R., 1959, Aspects of carbonate sedimentation: Journal of the Geological Society of Australia, v. 6, p. 1–10.

Anadón, P., and Utrilla, R., 1993, Sedimentology and isotope geochemistry of lacustrine carbonates of the Oligocene Campins Basin, north-east Spain: Sedimentology, v. 40, p. 699–720.

Arvidson, R. S., ms, 1998, The kinetics of dolomite precipitation with application to changes in seawater saturation state over the past 100 Ma: Ph.D. thesis, Honolulu, The University of Hawaii, 320 p.

Arvidson, R. S., and Mackenzie, F. T., 1997, Tentative kinetic model for dolomite precipitation rate and its application to dolomite distribution: Aquatic Geochemistry, v. 2, p. 273–298.

Badiozamani, K., 1973, The Dorag dolomitization model-application to the Middle Ordovician of Wisconsin: Journal of Sedimentary Petrology, v. 43, p. 965–984.

Baker, P. A., and Burns, S. J., 1985, Occurrence and formation of dolomite in organic-rich continental margin sediments: American Association of Petroleum Geologists Bulletin, v. 69, p. 1917–1930.

Baltzer, F., Kenig, F., Biochard, R., Plaziat, J. C., and Purser, B. H., 1994, Organic matter distribution, water circulation and dolomitization beneath the Abu Dhabi Sabkha (United Arab Emirates), *in* Purser, B., Tucker, M., and Zenger, D., editors, Dolomites: A volume in honour of Dolomieu: International Association of Sedimentologists Special Publication no. 21: Oxford, Blackwell, p. 409–427.

Bevington, P. R., and Robinson, D. K., 1992, Data Reduction and Error Analysis for the Physical Sciences, 2nd edition: New York, McGraw-Hill, Inc., 328 p.

Bischoff, W. D., ms, 1985, Magnesian calcites; physical and chemical properties and stabilities in aqueous solution of synthetic and biogenic phases: Ph.D. thesis, Northwestern University, Evanston, 144 p.

Brady, P. V., Krumhansl, J. L., and Papenguth, H. W., 1996, Surface complexation clues to dolomite growth: Geochimica et Cosmochimica Acta, v. 60, p. 727–731.
Busenberg, E., and Plummer, L. N., 1986, A comparative study of the dissolution and crystal growth kinetics of calcite and aragonite, *in* Mumpton, F. A., editor, Studies in Diagenesis: U. S. Geological Survey Bulletin B 1578, p. 139–168.
Calvo, J. P., Jones, B. F., Bustillo, M., Fort, R., Alonso-Zarza, A. M., and Kendall, C., 1995, Sedimentology and geochemistry of carbonates from lacustrine sequences in the Madrid Basin, Central Spain: Chemical Geology, v. 123, p. 173–191.
Carballo, J. D., Land, L. S., and Miser, D. E., 1987, Holocene dolomitization of supratidal sediments by active tidal pumping, Sugarloaf Key, Florida: Journal of Sedimentary Petrology, v. 57, p. 153–165.
Chai, L., Navrotsky, A., and Reeder, R. J., 1995, Energetics of calcium-rich dolomite: Geochimica et Cosmochimica Acta, v. 59, p. 939–944.
Compton, J. S., 1988, Degree of supersaturation and precipitation of organogenic dolomite: Geology (Boulder), v. 16, p. 318–321.
Deffeyes, K. S., Lucia, F. J., and Weyl, P. K., 1965, Dolomitization of recent and Plio-Pleistocene sediments by marine evaporite water on Bonaire, Netherland Antilles, *in* Pray, L. C., and Murray, R. C., editors, Dolomitization and Limestone Diagenesis: A Symposium: Society of Economic Paleontologists and Mineralogists Publication no. 13, p. 71–88.
Folk, R. L., and Land, L. S., 1975, Mg/Ca ratio and salinity: Two controls over crystalization of dolomite: American Association of Petroleum Geologists Bulletin, v. 59, p. 60–68.
Gaines, A. M., ms, 1968, An Experimental Investigation of the Kinetics and Mechanism of the Formation of Dolomite: Ph.D. thesis, Chicago, The University of Chicago, 83 p.
Goldsmith, J. R., 1983, Phase relations of rhombohedral carbonates, *in* Reeder, R. J., editor, Carbonates: Mineralogy and Chemistry: Mineralogical Society of America, Reviews in Mineralogy, v. 11, 2nd edition, p. 49–76.
Graf, D. L., Eardley, A. J., and Shimp, N. F., 1961, A preliminary report on magnesium carbonate formation in Glacial Lake Bonneville: Journal of Geology, v. 69, p. 219–223.
Graf, D. L., and Goldsmith, J. R., 1956, Some hydrothermal syntheses of dolomite and protodolomite: Journal of Geology, v. 64, p. 173–186.
Hardie, L. A., 1996, Secular variation in seawater chemistry: An explanation for the coupled secular variation in the mineralogies of marine limestones and potash evaporites over the past 600 m.y.: Geology (Boulder), v. 24, p. 279–283.
Helgeson, H. C., Kirkham, D. H., and Flowers, G. C., 1981, Theoretical prediction of the thermodynamic behavior of aqueous electrolytes at high pressure and temperatures: IV. Calculation of activity coefficients, osmotic coefficients, and apparent molal and standard and relative partial molal properties to 600°C and 5 KB: American Journal of Science, v. 281, p. 1249–1516.
Johnson, J. W., Oelkers, E. H., and Helgeson, H. C., 1992, SUPCRT92: A software package for calculating the standard molal thermodynamic properties of minerals, gases, aqueous species, and reactions from 1 to 5000 bar and 0 to 1000°C: Computers & Geosciences, v. 18, p. 899–947.
Jones, B. F., 1961, Zoning of saline minerals at Deeps Springs Lake, California: Short Papers in the Geological Sciences: U. S. Geological Survey Professional Paper 421, p. B199–B202.
——— 1965, The hydrology and mineralogy of Deep Springs Lake, Inyo County, California: Closed-Basin Investigations: U. S. Geological Survey Professional Paper 502-A, p. A1–A56.
Katz, A., and Matthews, A., 1977, The dolomitization of $CaCO_3$, an experimental study at 252–295°C: Geochimica et Cosmochimica Acta, v. 41, p. 297–308.
Kazmierczak, T. F., Tomson, M. B., and Nancollas, G. H., 1982, Crystal growth of calcium carbonate. A controlled composition kinetic study: Journal of Physical Chemistry, v. 86, p. 103–107.
Kelts, K., and McKenzie, J., 1982, Diagenetic dolomite formation in quaternary anoxic diatomaceous muds of Deep Sea Drilling Project Leg 64, Gulf of California, *in* Curray, J. R., Moore, D. G., and others, editors, Initial Reports of the Deep Sea Drilling Project, v. 64: Washington, D.C., U.S. Government Printing Office, p. 553–569.
Kharaka, Y. K., Gunter, S. D., Aggarwal, P. K., Perkins, E. H., and DeBraal, J. D., 1988, SOLMINEQ.88: A computer program for geochemical modeling of water-rock interactions: U. S. Geological Survey Water-Resources Investigations Report 88-4227, 420 p.
Land, L. S., 1973, Holocene meteoric dolomitization of Pleistocene limestones, North Jamaica: Sedimentology, v. 20, p. 411–424.
——— 1985, The origin of massive dolomite: Journal of Geological Education, v. 33, p. 112–125.
——— 1985, Failure to precipitate dolomite at 25°C from dilute solution despite 1000-fold oversaturation after 32 years: Aquatic Geochemistry, v. 4, p. 361–368.
Levenspiel, O., 1972, Chemical Reaction Engineering: New York, John Wiley & Sons, 578 p.
Lippmann, F., 1973, Sedimentary Carbonate Minerals, Minerals, Rocks and Inorganic Materials, Monograph Series of Theoretical and Experimental Studies, v. 4: Berlin, Springer-Verlag, 228 p.
Mackenzie, F. T., Bischoff, W. D., Bishop, F. C., Loijens, M., Schoonmaker, J., and Wollast, R., 1983, Magnesian calcites: Low temperature occurrence, solubility and solid-solution behavior, *in* Reeder, R. J., editor, Carbonates: Mineralogy and Chemistry: Reviews in Mineralogy, v. 11, 2nd edition, p. 97–144.
Malone, M. J., Baker, P. A., and Burns, S. J., 1996, Recrystallization of dolomite: An experimental study form 50–200°C: Geochimica et Cosmochimica Acta, v. 60, p. 2189–2207.
Mazzullo, S. J., Bischoff, W. D., and Teal, C. S., 1995, Holocene shallow-subtidal dolomitization by near-normal seawater, northern Belize: Geology (Boulder), v. 23, p. 341–344.
Middelburg, J. J., de Lange, G. J., and Kreulen, R., 1990, Dolomite formation in anoxic sediments of Kau Bay, Indonesia: Geology (Boulder), v. 18, p. 399–402.

Morse, J. W., and Mackenzie, F. T., 1990, Geochemistry of Sedimentary Carbonates, Vol. 48 of Developments in Sedimentology: Amsterdam, Elsevier, 707 p.
Noyes, R. M., 1962, Thermodynamics of ion hydration as a measure of effective dielectric properties of water: Journal of the American Chemical Society, v. 84, p. 513–522.
Peterson, M. N. A., Bien, G. S., and Berner, R. A., 1963, Radiocarbon studies of recent dolomite from Deep Spring Lake, California: Journal of Geophysical Research, v. 68, p. 6493–6505.
Press, W. H., Teukolsky, S. A., Vetterling, W. T., and Flannery, B. P., 1994, Numerical Recipes in Fortran: The Art of Scientific Computing, 2nd edition: Cambridge, Cambridge University Press, 963 p.
Reed, M. H., 1982, Calculation of multicomponent chemical equilibria and reaction processes in systems involving minerals, gases and an aqueous phase: Geochimica et Cosmochimica Acta, v. 46, p. 513–528.
Reed, M., and Spycher, N., 1984, Calculation of pH and mineral equilibria in hydrothermal waters with application to geothermometry and studies of boiling and dilution: Geochimica et Cosmochimica Acta, v. 48, p. 1479–1492.
Shiraki, R., and Brantley, S. L., 1995, Kinetics of near-equilibrium calcite precipitation at 100°C: An evaluation of elementary reaction-based and affinity-based rate laws: Geochimica et Cosmochimica Acta, v. 59, p. 1457–1471.
Shock, E. L., Oelkers, E. H., Johnson, J. W., Sverjensky, D. A., and Helgeson, H. C., 1992, Calculation of the thermodynamic and transport properties of aqueous species at high pressures and temperatures: Effective electrostatic radii, dissociation constants and the standard partial molal properties to 1000°C and 5 kbar: Journal of the Chemical Society: Faraday Transactions, v. 88, p. 803.
Stanley, S. M., and Hardie, L. A., 1998, Secular oscillations in the carbonate mineralogy of reef-building and sediment-producing organisms driven by tectonically forced shifts in seawater chemistry: Palaeogeography, Palaeoclimatology, Palaeoecology, v. 144, p. 3–19.
Tanger, J. C., and Helgeson, H. C., 1988, Calculation of the thermodynamic and transport properties of aqueous species at high pressures and temperatures: Revised equation of state for the standard partial molal properties of ions and electrolytes: American Journal of Science, v. 288, p. 19–98.
Vasconcelos, C., and McKenzie, J. A., 1997, Microbial mediation of modern dolomite precipitation and diagenesis under anoxic conditions (Lagoa Vermelha, Rio De Janeiro, Brazil): Journal of Sedimentary Petrology, v. 67, p. 378–390.
von der Borch, C. C., Rubin, M., and Skinner, B., 1964, Modern dolomite from South Australia: American Journal of Science, v. 262, p. 1116–1118.
Wells, A., 1962, Recent dolomite in the Persian Gulf: Nature (London), v. 194, p. 274–275.
Wenk, H.-R., and Meisheng, H., 1993, Partially disordered dolomite: Microstructural characterization of Abu Dhabi sabkha carbonates: American Mineralogist, v. 78, p. 769–774.
Worley, T. J., 1992, EQ3NR, A computer program for geochemical aqueous speciation-solubility calculations: Theoretical manual, user's guide, and related documentation (version 7.0): Lawrence Livermore National Laboratory, UCRL-MA-110662 PT III.